Chapter 6

Diphenyltin^{IV} dithiocarbamate macrocyclic complexes bearing varied linkers: Synthesis, spectral characterization, density functional theory and *in vitro* cytotoxic study

Abstract

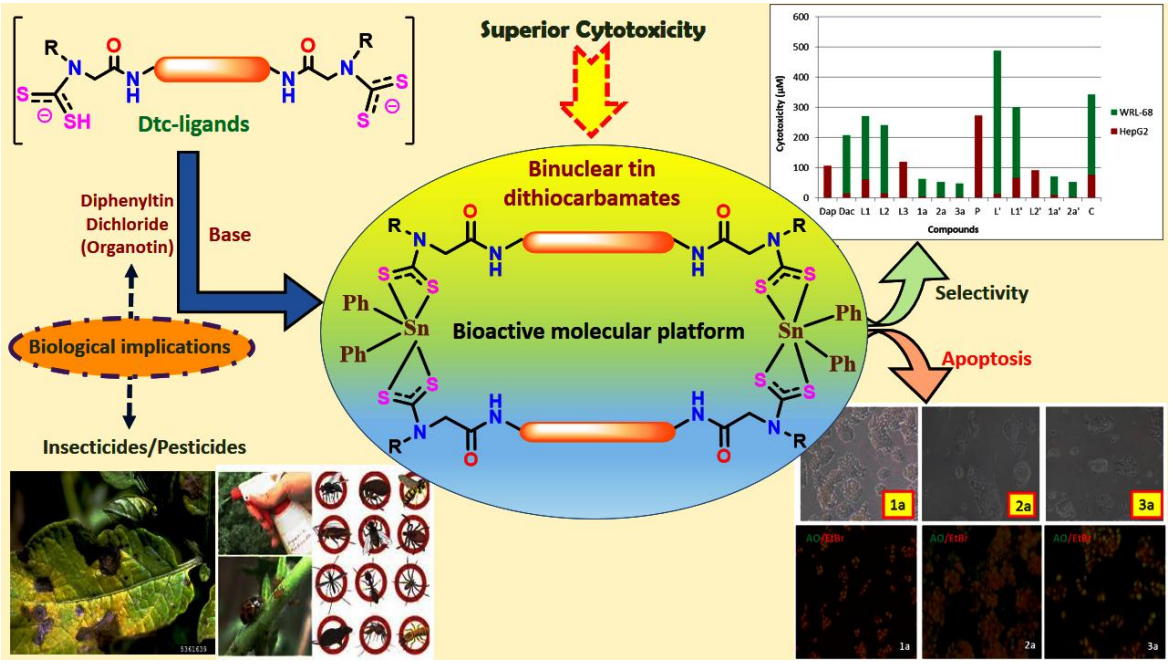

Five diamino precursors 4,4'-bis(2-(alkylamino)acetamido)diphenylsulfone (**L^1-L^3**) and 4,4'-bis(2-(alkylamino)acetamido)phenylene (**L^4-L^5**) were used to derive a new series of diphenyltin^{IV} dithiocarbamate complexes $[(Ph_2Sn^{IV})_2$-μ^2-bis{(κ^2S,S-$S_2CN(R)CH_2CONHC_6H_4)_2$ SO_2}] {R = Cy (**1**), ^{i}Pr (**2**), ^{n}Bu (**3**)} and $[(Ph_2Sn^{IV})_2$-μ^2-bis{(κ^2S,S-$S_2CN(R)CH_2CONH)_2C_6H_4$}] {R = Cy (**4**), ^{i}Pr (**5**)}. All the compounds have been characterized by relevant spectroscopic (^{1}H, ^{13}C, ^{1}H DOSY NMR, ESI MS, UV-visible absorption, IR) and thermogravimetric methods. Further density functional theory calculations have been carried out to reinforce the experimental data. MTT assay was

carried out on all the compounds to explore their *in vitro* cytotoxic ability against malignant human tumor Hep G2 (hepatoma) cell line. As anticipated the cytotoxic activity of their corresponding binuclear organotin^{IV} dithiocarbamate complexes **1-5** was boosted exceptionally to as high as 22 fold in **1** [3.32 ± 0.14 µM], 44 fold in **2** [1.77 ± 0.11 µM], 37 fold in **3** [2.02 ± 0.47 µM], 8 fold in **4** [8.72 ± 0.19 µM] and 29 fold in **5** [2.60 ± 0.67µM] compared to reference drug cisplatin [75.67 ± 0.51 µM]. Morphological proofs like shrinking of cells specifies the induction of apoptosis as part of the mechanism of action of these compounds which is further reinforced by the individual staining of the cells by acridine orange/ethidium bromide (AO/EB), however the mechanism and pathway of apoptosis needs to be established.

6.1 Introduction

One of the chief trepidations in research today is for the improvement of pharmacological competence to combat tumor disorders. Particularly in the field of oncology profound importance of metal complexes and organometallic compounds have been ascertained. [1] Cisplatin is one of the widely used cytotoxic agents, nevertheless its medical use is relentlessly restricted by acquired resistance and dose-limiting side-effects leading to treatment failure and clinical relapse. [2] The limitations of platinum chemotherapeutic metallopharmaceuticals lead to development towards non-platinum chemotherapeutics aiming the proficiency of such medications. Of these, organotins have developed as impending biologically active metallopharmaceuticals. The initial biocidal properties of triorganotin compounds like tripropyltin, triphenyltin and tributyltin were study by Van der Kerk et. al.[3] during 1954 and further reports suggest that these compounds successfully battle the parasite that roots for schistosomiasis in man.[4, 5] The late blight on potatoes and the leaf spot in sugar beets are known to be treated successfully by triphenyltin compounds as important agricultural fungicides.[6] Besides, the crucial role of organotin compounds as potent anti-tumourigenic agents both *in vitro* and *in vivo* has also been established. In this connection, Gielen and his coworkers have published a series of papers in recent past.[7-9] Apoptotic inducing character of organotin^{IV} compounds

[10-12] escalates their significance in cancer chemotherapy and thereby they occupy an important place in cancer chemotherapy reports.[10] P.J. Blower described thirty interesting inorganic pharmaceuticals, four of which are tin compounds.[13] Indeed, organotin moiety is crucial for cytotoxicity, the sulphur donor ligand plays a key role in transporting and presenting the molecule to the target and resisting untimely exchange with biomolecules.[14] Several di(4-cyanobenzyl)tin^{IV} dithiocarbamates exhibited very high activity against five human tumour cell lines.[15] Owing to the acidity observed in solid tumours due to anaerobic fermentation of glucose secreting lactic acid in tumour tissue [16] the apparently seen improved therapeutic index of sulfur containing complexes under acidic conditions[17] explains the enhanced cytotoxic activity against human tumour cell lines. The exact mechanisms by which these compounds control cell proliferation is not much known, however few reports claim macromolecular synthesis and the energy metabolism of mitochondria appear to be the plausible targets.[18-20] Other factors like ease of synthesis and effectual binding ability of dithiocarbamate ligands to eclectic array of metal ions present in different oxidation states of transition/non transition metal and organometallic building blocks improves the prospects to enhance the structural modifications of anti-tumor organotin compounds.[21-22] By a suitable choice of the ligand framework and N-substituents of the secondary amine precursors, Tiekink and others have proficiently used this system to design copious monometallic oganotin^{IV} dithiocarbamate complexes with several structural features that have shown numerous applications in material science and in medicinal chemistry.[22-27] In the light of great success of organic macrocyclic compounds in medicinal chemistry and significant role of sulfur donor ligands in biological progressions (vide supra), we have solely explored the cytotoxic potential of metallomacrocyclic dithiocarbamate complexes only recently.[28-30] Considering the appreciable *in vitro* cytotoxic properties of these compounds, especially organotin^{IV} dithiocarbamates macrocycles,[28] here we report a facile synthetic procedure, in depth spectroscopic characterization, computational studies and cytotoxic activity against human cancer cell lines HEPG2 (hepatoma) of a series of binuclear organotin^{IV} dithiocarbamate complexes $[(Ph_2Sn^{IV})_2\text{-}\mu^2\text{-bis}\{(\kappa^2S,S\text{-}S_2CN(R)CH_2CONHC_6H_4)_2SO_2\}]$ {R = Cy (**1**), ^{i}Pr (**2**), ^{n}Bu (**3**)} and $[(Ph_2Sn^{IV})_2\text{-}\mu^2\text{-bis}\{(\kappa^2S,S\text{-}S_2CN(R)CH_2CONH)_2C_6H_4\}]$ {R = Cy (**4**), ^{i}Pr (**5**)}. The presence of more than one organotin center in the

functionalized macrocyclic compounds **1-5** appears to exhibit higher effectiveness and specificity towards cytotoxicity.

6.2 Experimental Section

6.2.1 Instrumentations

Melting points were recorded in open capillaries and these are uncorrected. Thin layer chromatography (TLC) was performed on Merck 60 F254 aluminum coated plates to monitor the progress of reaction. ESI MS were obtained on AB SCIEX 3200 Q TRAP LCMS instrument. Infrared (KBr pellets) spectra were recorded in the 4000-400 cm^{-1} range using a Perkin-Elmer FT-IR spectrometer. ^{1}H, ^{13}C and DOSY NMR spectra were obtained on a Bruker AV-III 400 MHz spectrometer in DMSO-d^6 solvent and chemical shifts are reported in parts per million (ppm). UV-visible absorption spectra were recorded on a Perkin Elmer Lambda 35 UV-visible spectrophotometer. Fluorescence spectra were recorded on JASCO make spectrofluorometer model FP-6300. Thermogravimetric analysis was carried out on SII TG/DTA 6300 under flowing N_2 with a heating rate of 10 °C min^{-1}.

6.2.2 Synthesis of binuclear diphenyltin^{IV} dithiocarbamate macrocyclic complexes (1-5)

To a basic acetonitrile solution containing surplus amount of NaOH (~3 equivalent; ~ 0.060 g) $L^{\mathbf{1}}$ (0.263 g 0.5 mmol), $L^{\mathbf{2}}$ (0.223 g, 0.5 mmol), $L^{\mathbf{3}}$ (0.237 g, 0.5 mmol), $L^{\mathbf{4}}$ (0.193 g, 0.5 mmol) or $L^{\mathbf{5}}$ (0.153 mg, 0.5 mmol) and excess carbon disulfide (~10 equivalent; ~ 0.5 ml) were added. The reaction mixture was allowed to stir for 12 hours at room temperature wherein a change in colour from colourless to pale yellow was observed. To this mixture, diphenyltin dichloride (189.1 mg, 0.55 mmol) was added with rigorous stirring and the reaction was further allowed to continue for 12 h at room temperature. The residue was filtered in a glass sintered crucible and washed numerous times with distilled acetonitrile followed by n-hexane and diethyl ether. The off-white

residue in case (in the case of **1** and **2**) and yellow residue (in the case of **3-5**) was vacuum dried, stored under N_2 atmosphere and taken for analysis.

[(Ph_2Sn^{IV})$_2$-μ^2-bis{(κ^{2}S,S-$S_2CN(Cy)CH_2CONHC_6H_4)_2SO_2$}] (1). White; MW: 1899.73; Yield: 393 mg, 83%; m.p. 194°C dec.; ESI MS: 1899.4 (M^+); FTIR (KBr disc, cm^{-1}): 3491.58m, broad, 3044.63w, 2930.01s, 2853.90s, 1705.00 vs, 1590.79 vs, 1522.43s, 1498.74m, 1402.43s, 1310.30s, 1242.21m, 1151.23s, 1105.54s, 1071.02m, 1010.19m, 966.13w, 916.02w, 891.81w, 837.91m, 728.32m, 694.39m, 604.77m, 574.29w, 529.74w, 448.17m. ^{1}H NMR (DMSO-d_6, 400 MHz): δ (ppm) 10.672 (s, 4H, CON*H*); 7.840-7.318(m, 36H, *Ph*); 4.552 (s, 8H, NCH_2CO); 4.356 (C*H* of Cy); 2.08 (br, s), 1.783-1.071 (m, 40H, *Cy*). ^{13}CNMR (400 MHz, DMSO-d_6): δ ppm: 206.92 **(-N^{13}*C*S$_2$)**, 179.80, 171.00 (*C*=O), 143.71, 136.23, 135.66, 134.70 (*C*-N), 130.71, 130.53, 129.52, 129.26 (Sn– *Ph*), 128.90, 128.55, 127.97, 119.73, 119.42(*Ph*), 56.60 (N*C*H_2CO), 52.86 (*C*H of *Cy*), 29.93, 29.57, 25.57, 25.33, 25.22, 25.07, 24.59 (*C*H_2 of Cy).

[(Ph2Sn^{IV})$_2$-*μ^2*-bis-{(*κ^{2}S,S*-$S_2CN(^iPr)CH_2CONHC_6H_4)_2SO_2$}] (2). White; MW: 1739.47; Yield: 386 mg, 89%; m.p. 162°C dec.; FTIR (KBr disc, cm^{-1}) 3374.82m, 3047.71m, 2976.66m, 1727.93, 1711.57m, 1590.17vs, 1526.29s, 1496.59m, 1467.30m, 1403.00s, 1367.77w, 1309.24s, 1254.39m, 1183.95m, 1146.32s, 1105.65s, 1071.60s, 1020.14w, 995.69m, 944.83w, 908.92w, 839.56s, 693.12m, 620.27m, 571.21m, 544.72m, 449.44m. ^{1}H NMR (DMSO-d_6, 400 MHz): δ (ppm) 10.699(s, 4H, CON*H*); 7.933-7.405(m, 36H, *Ph*); 4.829, 4.557 (s, 8H, NCH_2CO); 4.332 (s, 4H, C*H* of ^{i}Pr); 1.313-1.110 (d, 24H, CH_3). ^{13}CNMR (400 MHz, DMSO-d_6): δ ppm: 172.00 (*C*=O), 135.99, 134.48 (*C*-N), 130.54, 129.32 (Sn– *Ph*), 128.90, 128.61, 128.24, 119.67, 113.41 (*Ph*), 48.69 (N*C*H_2CO), 48.13 (CH of ^{i}*Pr*), 22.15, 19.94, 19.51(CH_3 of ^{i}*Pr*).

[(Ph2Sn^{IV})$_2$-*μ^2*-bis-{(*κ^{2}S,S*-$S_2CN(^nBu)CH_2CONHC_6H_4)_2SO_2$}](3). Yellow; MW: 1795.58; Yield: 421 mg, 94%; m.p. 196°C dec. FTIR (KBr disc, cm^{-1}): 3108.65w, 3045.52w, 2928.12m, 2866.54m, 1704.50s, 1645.59w, 1590.45s, 1527.48s, 1429.70m, 1402.46m, 1364.62w, 1314.37s, 1254.29m, 1223.68m, 1150.79s, 1107.23s, 1070.62w, 998.45m, 937.65w, 836.64s, 727.54m, 693.95m, 635.55w, 550.05w, 448.70m. ^{1}H NMR (DMSO-d_6, 400 MHz): δ (ppm)

10.767(s, 4H, CON*H*); 8.022-7.300 (m, 36H, *Ph*); 4.720 (s, 8H, NCH_2CO); 3.845 (s, 8H, NCH_2 of ^{n}*Bu*); 2.926 (m, 8H, CH_2 of ^{n}*Bu*); 1.617 (m, 8H, CH_2 of ^{n}*Bu*); 1.326-1.201 (m, 8H, CH_2 of ^{n}*Bu*); 0.915-0.820 (m, 12H, CH_3 of ^{n}*Bu*). ^{13}CNMR (400 MHz, DMSO-d_6): δ ppm: 202.132 **(-N^{13}*C*S$_2$)**, 170.82, 166.32 (*C*=O), 136.28, 136.02, 135.74 (*C*-N), 129.26 (Sn– *Ph*), 128.93, 128.80, 128.54, 128.38, 119.52, 113.44 (*Ph*), 58.31, 57.41 (N*C*H$_2$CO), 53.12 (NCH$_2$ of ^{n}*Bu*), 28.84, 28.78, 19.88, 19.79 (*C*H$_2$ of ^{n}*Bu*), 14.13, 14.09 (*C*H$_3$ of ^{n}*Bu*).

[(Ph2Sn^{IV})$_2$-*μ*^{2}-bis-{(*κ*^{2}*S*,*S*-S$_2$CN(Cy)CH$_2$CONH)$_2$C$_6$H$_4$}] (4). Yellow; MW: 1619.42, Yield: 347 mg, 86%; m.p. 191°C dec.; ESI MS: 1619.0 (M^+); FTIR (KBr disc, cm^{-1}): 3410.43m, 2931.01s, 2853.98m, 1688.00s, 1607.57s, 1537.29m, 1451.36s, 1233.35m, 1164.24m, 1008.00m, 783.33w, 729.08m, 692.96s, 582.00w, 448.48w. ^{1}H NMR (DMSO-d_6, 400 MHz): δ (ppm) 10.404 (s, 4H, CON*H*); 7.995-7.177(m, 28H, *Ph*); 4.752 (s, 8H, NCH_2CO); 4.353 (m, br, 4H, C*H* of Cy); 1.967-0.819 (m, 40H, *Cy*). ^{13}CNMR (400 MHz, DMSO-d_6): δ ppm: 139.72, 136.24, 136.08, 134.84 (*C*-N) 129.44, 129.17, 128.91(Sn– *Ph*), 128.46, 128.10, 114.35, 110.11(*Ph*), 56.56 (N*C*H$_2$CO), 52.90 (*C*H of *Cy*), 31.64, 29.95, 25.63, 25.12, 24.53 (*C*H$_2$ of Cy).

[(Ph2Sn^{IV})$_2$-*μ*^{2}-bis-{(*κ*^{2}*S*,*S*-S$_2$CN(*^{i}Pr*)CH$_2$CONH)$_2$C$_6$H$_4$}] (5). Yellow MW: 1459.16; Yield: 302 mg, 83%; m.p. 193°C dec.; ESI MS: 1483.5 (M+Na); FTIR (KBr disc, cm^{-1})**:** 3417.99m, 3063.35w, 2976.15w, 1679.60s, 1606.32s, 1536.97m, 1429.59s, 1304.57w, 1221.10m, 1169.43w, 1071.60m, 996.98m, 779.01m, 727.65s, 694.07s, 580.00m, 447.13m. ^{1}H NMR (DMSO-d_6, 400 MHz): δ (ppm) 10.510, 10.321 (s, 4H, CON*H*); 7.945-7.299 (m, 28H, *Ph*); 4.591, 4.493 (s, 8H, NCH_2CO); 4.362 (s, 4H, C*H* of ^{i}Pr); 1.220-0.995 (d, 24H, CH_3). ^{13}CNMR (400 MHz, DMSO-d_6): δ ppm: 171.29 (*C*=O), 136.19, 136.01 (*C*-N), 129.21 (Sn–*Ph*); 128.50, 119.67 (*Ph*); 53.13, 51.81 (N*C*H$_2$CO), 48.65, 48.02 (CH of ^{i}*Pr*), 22.86, 20.10, 19.55 (CH$_3$ of ^{i}*Pr*).

6.2.3 *In vitro* cytotoxicity study

6.2.3.1. Cell line and culture

HepG2 and WRL-68 cell lines were procured from the National Centre for Cell Science, Pune; pre-cultured in DMEM medium (supplemented with 10% fetal bovine serum (FBS) and 1% antibiotics) in tissue culture flasks. Cultured cells were incubated at 37°C in CO_2 incubator containing 5% CO_2. Culture medium was changed every second day and cell growth was monitored microscopically. Cells were regularly trypsinized and subcultured into new flasks.

6.2.3.2. MTT assay for cell viability/ proliferation

MTT assay was performed for testing cytotoxicity potential of test compounds and their ensuing complexes. HepG2 cells were plated (10^3cells / well in 100 µL of medium) in a 96 well plate in their exponential growth phase, for 24 hr. Test compounds were prepared in 5% DMSO and cells were exposed to different concentration of test compounds (6.25µg/ml, 12.5µg/ml, 25µg/ml, 50µg/ml and 100 µg/ml) for 24 hrs. Post incubation media was removed and cells were incubated with 10µL of MTT reagent (5mg/ml) at 37^0C for 4hrs. DMSO was used to solubilize formazan crystals, produced by only viable cells. The optical density was measured at 540nm by an ELISA reader (BIOTEK ELX800 Universal Microplate Reader).[52] Percentage cytotoxicity was calculated against control (media with DMSO only) for all the test compounds.

6.2.3.3. Statistical Analysis for Determination of IC_{50}

Data obtained was analyzed in Prism/ OriginPro8 for standard error and probit analysis. The percent cytotoxicity index (% CI) was calculated as follows:

% CI= [1− (OD of treated cells/ ODof control cells)] × 100 %

where, CI= cytotoxicity index, OD= optical density.

A plot of % CI versus concentration was obtained from the experimental data for each set of experiments. The values of IC_{50} (50% growth inhibition of cell) were determined from the graph.

6.2.3.4. Assessment of apoptosis AO/EtBr staining

Cells were grown in 24 well-plate (5 x 10^5) and then incubated in a CO_2 incubator at 37^0C. Cells were dosed with IC50 concentration of compounds for 24 hrs after which, cells were washed with PBS and stained with 200µl of AO-EtBr mixture (100µg/ml AO: 100µg/ml EtBr). Cells were observed under FLoid™ Cell Imaging Station (Life Technologies) fluorescent microscope at 20X magnification.[53]

6.3. Result and Discussion

6.3.1. Syntheses and characterization

The promising exploration of diamino/bisimine organic precursors bearing polyaromatic hydrocarbons as well as bimetallic dithiocarbamate self-assemblies[28-31] against several human cancer cell lines has enthused us to synthesize a new series of binuclear Ph_2Sn^{IV} dithiocarbamate macrocyclic compounds $[(Ph_2Sn^{IV})_2$-µ^2-bis{(κ^{2}S,S-$S_2CN(R)CH_2CONHC_6H_4)_2SO_2$}] {R = Cy (**1**), ^{i}Pr (**2**), ^{n}Bu (**3**)} and $[(Ph_2Sn^{IV})_2$-µ^2-bis{(κ^{2}S,S-$S_2CN(R)CH_2CONH)_2C_6H_4$}] {R = Cy (**4**), ^{i}Pr (**5**)} bearing biologically active polar amide, sulfone, polyaromatic hydrocarbon, dithiocarbamate and Ph_2Sn^{IV} groups in the macrocyclic framework. Our recently reported diamino precursors 4,4'-bis(2-(alkylamino)acetamido)biphenylsulfone (**L^1-L^3**)[30] and 4,4'-bis(2-(alkylamino)acetamido) phenylene (**L^4-L^5**) [32] have been utilized further to derive these complexes. Thus, a facile one-pot reaction protocol involving self-assembly of the corresponding diamine **L^1–L^5** with CS_2 and Ph_2SnCl_2 affords access to **1-5** as shown in Scheme 1.

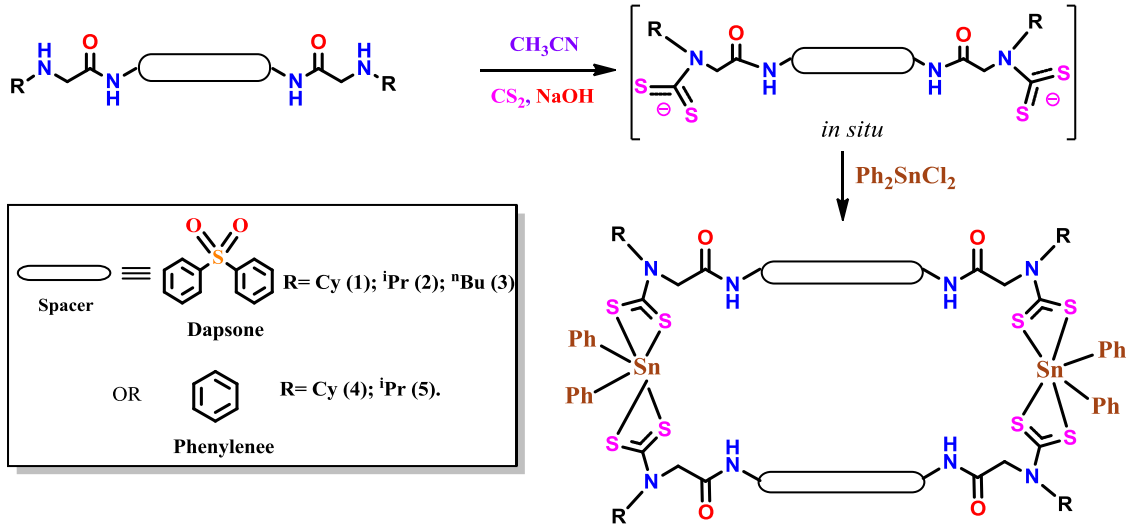

Scheme 1: One-pot synthetic protocol for binuclear Ph_2Sn^{IV} dithiocarbamate macrocycles **1-5**.

It is foreseen that the presence of various active pharmacophores (vide supra) on to a single molecular platform would provide admission to enhanced cytotoxicity with improved interactions of these compounds with various biomolecules. The newly synthesized compounds have been suitably characterized by relevant spectroscopy, thermogravimetric methods and DFT calculations have been performed on representative compound to reinforce the experimental outcomes.

6.3.2. NMR, Mass and IR spectral study

The nature of chelation of the dithiocarbamate ligand appears to be anisobidentate owing to the presence of IR bands in the range of 1498-1429 cm^{-1} due to ν(N–CSS) and 1070-1071 for νas(CSS) stretching vibrations. [33] The characteristic IR bands at 574-550 cm^{-1} and 448-449, attributable to Sn–C and Sn–S stretching vibrations support the formation of to Sn–C and Sn–S bonds in the macrocyclic self-assemblies (Annexure 4-8).The ESI-MS spectra of these complexes gave m/z molecular ions peaks at 1899.4, 1619.0 and 1483.5 for **1, 4** and **5** respectively which corresponds to either $[M^+]$ and [M+Na] molecular ions (Annexure 1-3). As anticipated, signals corresponding to methine/methylene groups of NCH–/NCH_2– substituents and methylene group of NCH_2CO linker in complexes **1-5** experienced substantial downfield displacements when

compared to the respective diamino precursors. Owing to the bulky size of the complexes as well as the facile conformational flexibiltity the self-assembled macrocyclic structures the assignment to every ^{1}H NMR signal becomes difficult. Importantly, The ^{13}C NMR spectra of representative complexes **1** and **3** showed a single distinct downfield resonance at δ 206 and 202 ppm associated with the N–CS_2 unit. [28, 30, 31] The occurrence of predicted signals and lack of signals corresponding to uncoordinated end groups in the NMR spectra of **1-5** ruled out the probability of formation of oligomers or coordination polymeric products. (Annexure 9, 10, 11, 12, 13, 14, 16, 19 and annexure 20) The ^{1}H DOSY NMR spectral analysis of complexes **1** (Fig. 1), **3, 4** and **5** (Annexure 3, 18 and annexure 21), unequivocally display the presence of only one type of species in solution and rule out the possibility of formation of oligomers or coordination polymers. The reasonably symmetric arrangement of phenyl groups in the coordination sphere of the central tin^{IV} atoms in solution can be ascertained by the appearance of single one set of NMR signals for both the phenyl groups of $Ph2Sn^{IV}$ in **1-5.** Specifically self-assembly of a distinct supramolecular arrangement is primarily decided by factors like stereo-electronic features of ligand framework,[34] metal center as well as thermodynamic conditions [35] along with progression of the reaction in opposition with polymerization. [36]

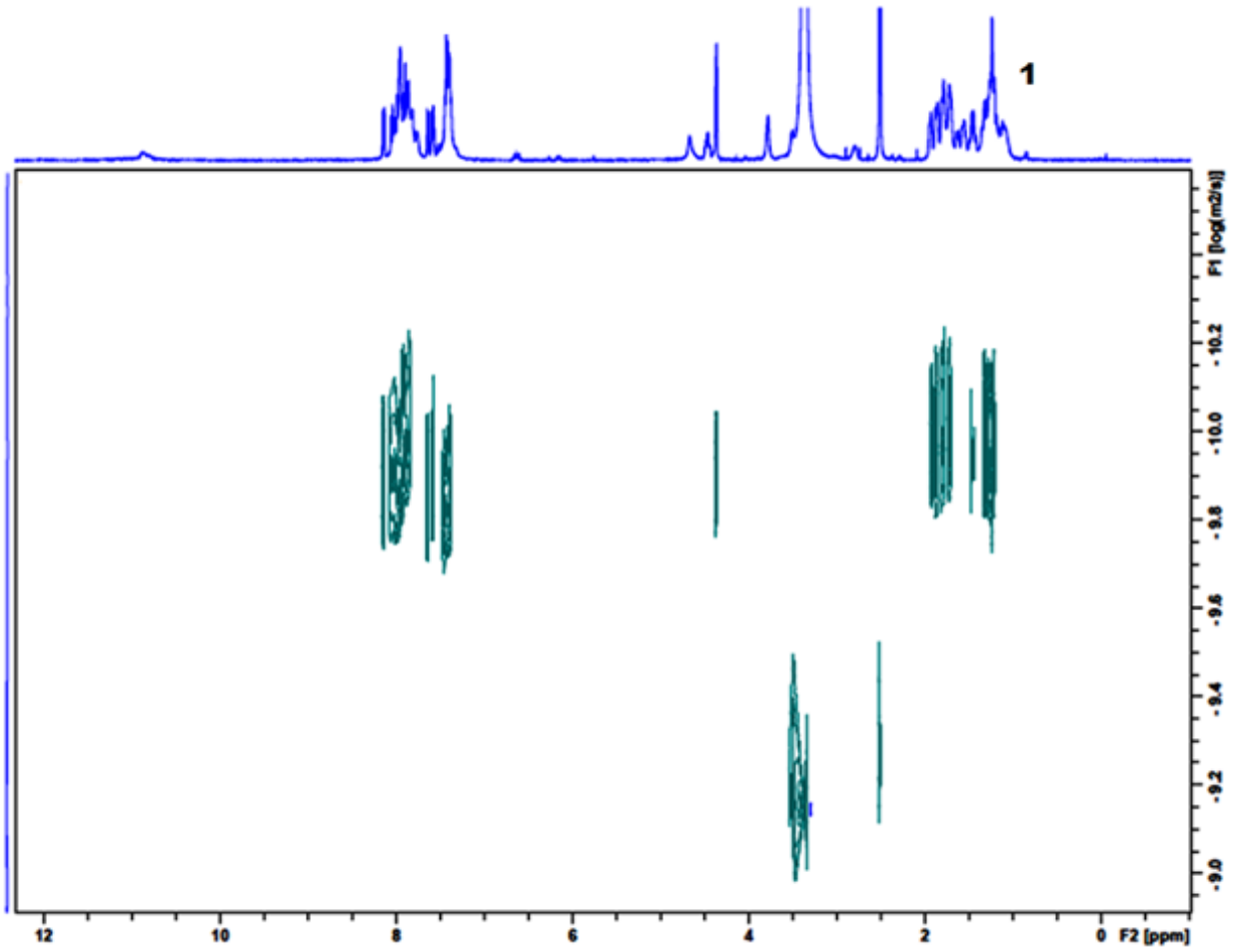

Fig. 1. DOSY NMR spectrum of **1**.

6.3.3. UV-visible absorption and emission spectral study

The UV–visible absorption spectra of $\mathbf{L^1}$-$\mathbf{L^5}$ display a single noticeable band at shorter wavelength of 290-309 nm, corresponding to $\pi \rightarrow \pi^*$ (phenyl) transitions, however, similar to the absorption behavior of diorganotin dithiocarbamate complexes, [37-40] complexes **1-5** reveal two main bands at 295-298 and 392-400 nm attributable to $\pi \rightarrow \pi^*$ (phenyl) and charge transfer transitions (Fig 2.), individually. Ligand precursors, $\mathbf{L^1}$, $\mathbf{L^4}$ and $\mathbf{L^5}$ display robust fluorescence emissions at 475, 291 and 275 nm from excited $\pi \rightarrow \pi^*$ transition states; on the other hand ligand precursors $\mathbf{L^1}$ and $\mathbf{L^3}$ show feeble emission

intensity upon excitation at their corresponding λmax values at room temperature. (Table 1)

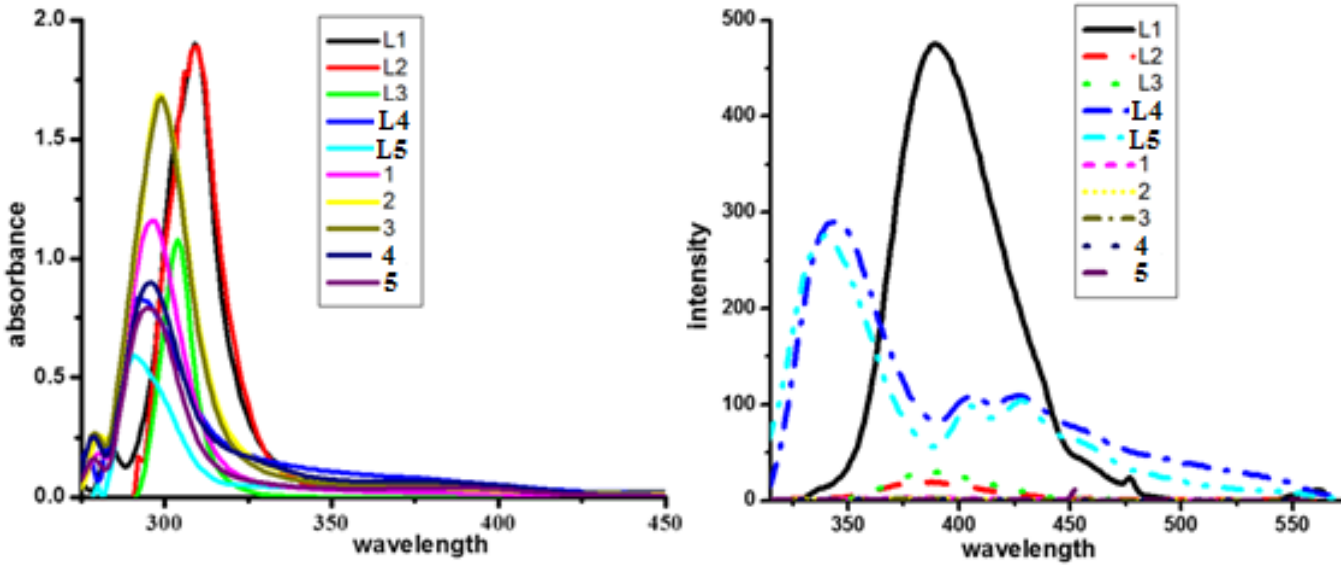

Fig. 2. UV-visible absorption spectra and Fluorescence spectra in DMF for 1mM **1-5** complexes.

Table 1. UV–visible absorption and emission spectral data for $\mathbf{L^1}$-$\mathbf{L^5}$ and **1-5** complexes.

Entry	λ_{max} nm(ε L $Mol^{-1}cm^{-1}$)	Wave number	Magnetic Moment μ_{eff}(BM)	Fluorescence spectral data (10^{-3} M DMF)	
				λ_{ex} nm	λ_{em}(nm) (Intensity)
$\mathbf{L^1}$	309(1900)π→π*	3236	dia	309	389 (475)
$\mathbf{L^2}$	309 (1890) π→π*	3236	dia	309	387(19)
$\mathbf{L^3}$	304 (1080)π→π*	3289	dia	304	387(30)
$\mathbf{L^4}$	292(820) π→π*	3424	dia	292	344(291)
$\mathbf{L^5}$	290(590) π→π*	3448	dia	290	339(275)
1	296(1150) π→π*	3378	dia	296	Non
	399 (10) dπ-pπ (CT)	2506			fluorescent
2	298(1690) π→π*	3355	dia	298	Non
	393(30) dπ-pπ (CT)	2544			fluorescent
3	298 (1660) π→π*	3355	dia	298	Non
	401 (40) dπ-pπ (CT)	2493			fluorescent
4	295 (890) π→π*	3389	dia	295	Non
	392 (50) dπ-pπ (CT)	2551			fluorescent
5	295 (790) π→π*	3389	dia	295	Non
	400 (30) dπ-pπ (CT)	2500			fluorescent

The binuclear Ph_2Sn^{IV} dithiocarbamate complexes **1-5** demonstrate non-fluorescent property and evidently the fluorescence of diamine precursors $\mathbf{L^1–L^5}$ is successfully quenched upon the formation of respective binuclear complexes with Ph_2Sn^{IV} which supports the presence of hexacoordinate tin^{IV} centers in **1-5**. Literature suggests penta-coordinated flavonoid $organotin^{IV}$ derivatives fluoresce strongly, whereas its hexa coordinated derivatives are non-fluorescent in nature. [40-43]

6.3.5. Thermogravimetric analysis (TGA)/differential thermal analysis (DTA) study

Under N_2 atmosphere thermogravimetric plots of complexes **1, 3, 4** and **5**, were recorded from room temperature to 550 °C at a heating rate of 10 °C/min. A multistage thermal degradation of the binuclear complexes **1, 3, 4** and **5** is observed from the analogous TGA curves which are undeniably accompanied by numerous endothermic and/or exothermic peaks in DTA curves. (Annexure 22-25) Maximum rate of degradation for these compounds were recorded on DTG curves at diverse temperatures. In all cases, the weight loss continues to 550°C and the TGA curves demonstrate a relatively greater thermal stability in **1, 3, 4** and **5**. Such a multistage thermal degradation pattern has formerly been recounted for a number of $organotin^{IV}$ dithiocarbamate complexes. [41-43]

6.3.5. Geometry Optimization

For a better understanding of the spectroscopic results, we carried out a full geometry optimization of macrocyclic binuclear tin dithiocarbamate complexes **1** (Fig. 3) using density functional theory (DFT) with B3LYP/LanL2DZ basis sets, respectively. The electronic structural parameters are found to be consistent with the X-ray data of closely related compounds. [44, 45] Loss of coplanarity associated with amide moiety along with distinct deviations in electronic structural parameters establishes the high flexibility of –$(CH_2CONHC_6H_5)_2SO_2$– linker. This factor plays a key role for improved interaction with various biomolecules. The optimized geometry of **1** demonstrates the formation of binuclear macrocyclic compounds with distorted octahedral geometry with cis–cis

arrangement of diphenyltin moieties connecting two tin centers through terminal dithiocarbamates.

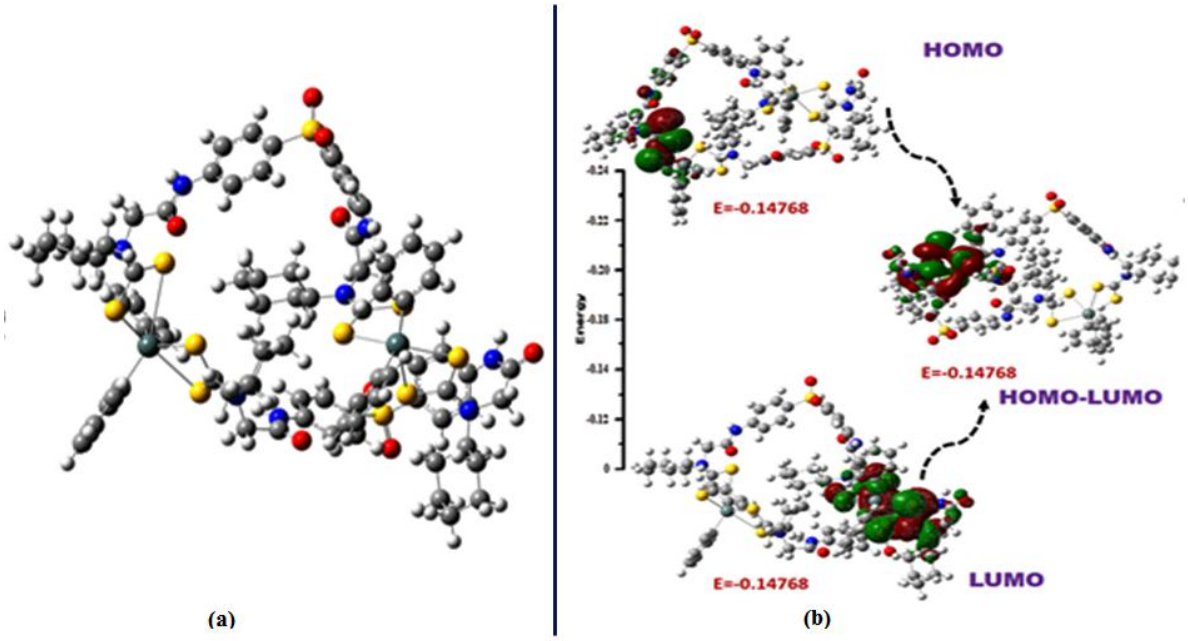

Fig. 3. (a) Optimized geometry for minimum energy conformation at B3LYP/LanL2DZ basis level and (b) Frontier molecular orbitals (Isovalue= 0.02) derived from DFT calculation at the B3LYP/LAN2DZ level for complex **1.**

Out of the four cyclohexyl groups in the macrocyclic architecture two of them are oriented within the 44-member molecular cavity as observed in the space-fill model of optimized geometry of **1** (fig. 4) . The substantial un-equality in the Sn–S bond distances (2.52–3.48 Å) and N–CS_2 bond distances (1.34–1.36 Å) exhibits the anisobidentate coordination mode of the –NCS_2 moieties. The bond angles for PhC–Sn–CPh associated with one of the Sn centres appear at 114.49° whereas bond angle for another Sn centre appeared at 103.27°, which are in concurrence with experimental results. [44, 45] The bond angle associated with C–SO_2–C shows a difference of 2.3° of the two linkers.

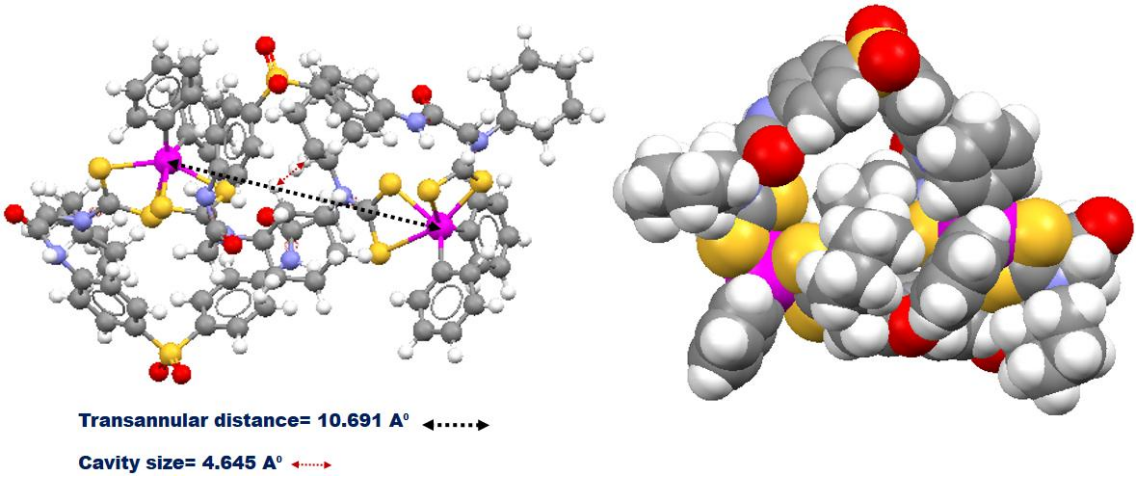

Fig. 4. Optimized geometry as space-filling model revealing a cavity generated by the macrocyclic architecture of dinuclear Ph_2Sn^{IV} dithiocarbamate complex **1**

The transannular Sn-Sn distances obtained from the optimized geometry of **1** (fig. 4) appear at 10.691 Å which is larger than their analogous systems.[46] The optimized geometry clearly reveals the orientation of the peripheral polar amide groups well outside the cavity of the macrocyclic complex enhancing the hydrogen bonding interactions with various biomolecules.[47-49] The electron density of highest occupied molecular orbital (HOMO) is restricted to the one of the coordinated dithiocarbamate moiety while lowest unoccupied molecular orbital (LUMO) is predominantly localized at one of the diphenyltin(IV) dithiocarbamate moieties. The λmax value for **1** obtained through computational investigations appears at 308 nm which is comparable to λmax (295 nm) obtained for **1** experimentally thus validating the authenticity of DFT studies.

6.3.6 *In vitro* cytotoxic activity

The compounds were studied for their *In vitro* cytotoxic prospective by MTT assay against the malignant tumor cell line HepG2 (Hepatoma). The outcomes were compared with the clinically used antineoplastic drug cisplatin [C]. The 50% inhibition concentration (IC50) readings attained after incubation for 24hrs for all the compounds against HepG2 cell line are abridged in Table 2 and Fig 5. The compounds exhibiting IC50 lower than Cisplatin were additionally screened for their activity on normal liver cell line (WRL-68) under analogous environments. The results demonstrated on both cell

lines clearly indicate the specificity of these compounds for cancer cells over normal cells. The first derivative (**Dac** IC50=14.40 ± 0.83 μM) of one of the lead compound dapsone (**Dap** IC50= 105.92 ± 0.80 μM) exhibits pronounced cytotoxicity against HepG2. Although **Dac** could not preserve the activity upon formation of its $\mathbf{L^1}$ (IC50=61.42 ± 0.28 μM) and $\mathbf{L^3}$ (IC50=118.19 ± 0.37 μM), derivatives, however the cytotoxicity of $\mathbf{L^1}$ and $\mathbf{L^3}$ is outstandingly enhanced upon formation of its diphenyltin^{IV} dithiocarbamate complexes **1** (IC50=3.32 ± 0.14μM), **2** (IC50=1.77 ± 0.11μM) and **3** (IC50=2.02 ± 0.47 μM) against HepG2 cell line. Unlike the activity of transition metal dithiocarbamate macrocyclic compounds derived from same set of ligands,[30] the activity of these organometallic macrocyclic compounds **1-3** are found to be much superior. The poor cytotoxicity demonstrated by the other lead compound phenylene (**P** IC50= 105.92 ± 0.80 μM) reported by us lately [32] was further improved in its corresponding chloro derivative (**L'** IC50= 12.68 ± 0.38 μM). However the activity further dropped upon formation of its $\mathbf{L^4}$ (IC50=64.98 ± 0.54 μM) and $\mathbf{L^5}$ (IC50=64.98 ± 0.54μM), derivatives. Conversely upon the formation of its corresponding diphenyl tin dithiocarbamate complexes **4** (IC50=8.72 ± 0.19 μM) and **5** (IC50=2.60 ± 0.67μM) the cytotoxic property of these tin containing compounds enhanced stupendously. Thus, as anticipated on incorporating the organotin moiety in the form of diphenyl tin in the presence of biologically relevant dithiocarbamate fragment within the same molecular platform the cytotoxicity of the corresponding binuclear tin dithiocarbamate complexes increased tremendously.

Table 2. IC_{50} values for entry **1-15** against HepG2 cancer cells.

Entry	Compounds	HepG2 IC50 in μM	WRL-68 IC50 in μM
1	4,4'-diaminodiphenylsulfone **(Dap)**	105.92 ± 0.80	-
2	4,4'-bis(2-chloroacetamido)diphenylsulfone **(Dac)**	14.40 ± 0.83	193.14 ± 0.44
3	4,4'-bis(2-(cyclohexylamino)acetamido)diphenylsulfone **($\mathbf{L^1}$)**	61.42 ± 0.28	208.98 ± 0.52
4	4,4'-bis(2-(isopropylamino)acetamido)diphenylsulfone **($\mathbf{L^2}$)**	13.70 ± 0.78	226.77 ± 0.18
5	4,4'-bis(2-(n-butylamino)acetamido)diphenylsulfone **($\mathbf{L^3}$)**	118.19 ± 0.37	-
6	$[(Ph2SnIV)_2$-μ^2-bis$\{(\kappa^2S,SS_2CN(Cy)CH_2CONHC_6H_4)_2SO_2]$**(1)**	3.32 ± 0.14	59.00 ± 0.24
7	$[(Ph2SnIV)_2$-μ^2-bis$\{(\kappa^2S,SS_2CN(^iPr)CH_2CONHC_6H_4)_2SO_2\}]$**(2)**	1.77 ± 0.11	50.67 ± 0.27
8	$[(Ph2SnIV)_2$-μ^2-bis-$\{(\kappa^2S,S$-$S_2CN(^nBu)CH_2CONHC_6H_4)_2\ SO_2\}]$**(3)**	2.02 ± 0.47	45.31 ± 0.34
9	m- diamino phenylene **(P)**	272.88 ± 0.29	-

10	4,4'-bis(2-chloroacetamido)phenylene **(L')**	12.68 ± 0.38	474.53 ± 0.15
11	4,4'-bis(2-(cyclohexylamino)acetamido)phenylene **(L^4)**	64.98 ± 0.54	234.59 ± 0.17
12	4,4'-bis(2-(isopropylamino)acetamido) phenylene **(L^5)**	89.88 ± 0.33	-
13	$[(Ph2SnIV)_2$-μ^2-bis-$\{(\kappa^2S,S$-$S_2CN(Cy)CH_2CONH)_2\ C_6H_4\}]$ **(4)**	8.72 ± 0.19	62.14 ± 0.21
14	$[(Ph2SnIV)_2$-μ^2-bis-$\{(\kappa^2S,S$-$S_2CN(^iPr)CH_2CONH)_2\ C_6H_4\}]$ **(5)**	2.60 ± 0.67	50.53 ± 0.17
15	Cisplatin **(C)**	75.67 ± 0.51	266.67 ± 0.15

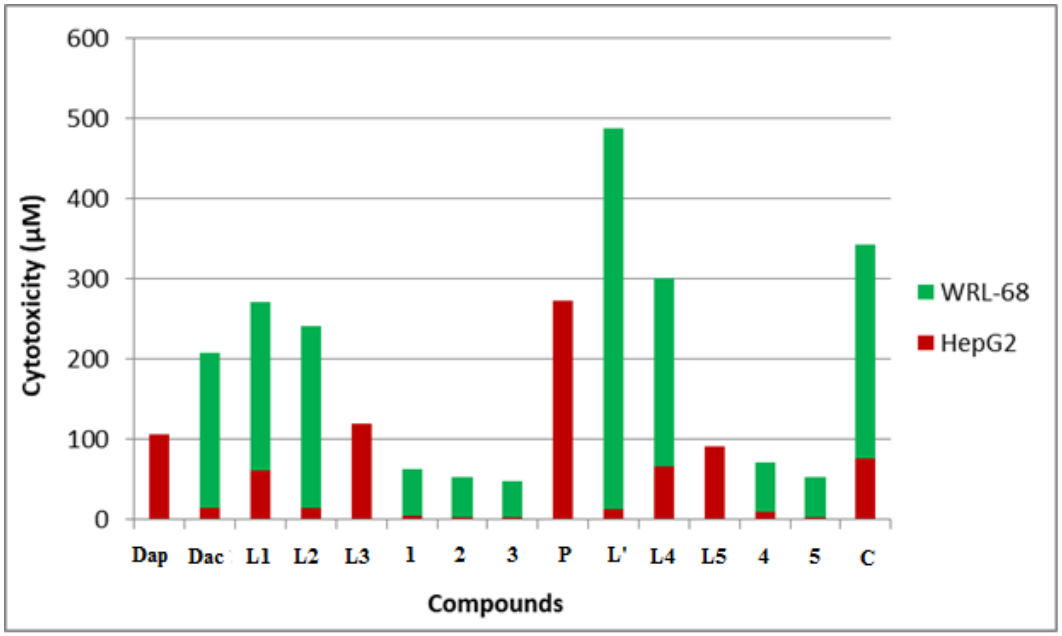

Fig. 5. Cytotoxic activity IC_{50} values (µM) for lead compounds, **L^1-L^5** and complexes **1-5**.

In initiation of cell death apoptosis is a key event and the most preferred pathway. [50] Apoptosis is a strongly regulated programmed cell death which plays a significant role in controlling the rate of cell death as well as that of cell division. It is also known to regulate the immune system, cell population in tissues, aging and many other physiological processes. The ability to selectively promote apoptosis in cancer cells while causing less or no damage to normal healthy cells. [51-52] is one of the prime factors to decide the worth of any cytotoxic drugs. This distinguishing property is precisely demonstrated by **Dac**, **L^1**, **L^2**, **1**, **2**, **3**, **L'**, **L^4**, **4** and **5** which targets exclusively cancerous cells HEPG2 and shows no major effect in normal liver cell line WRL-68.

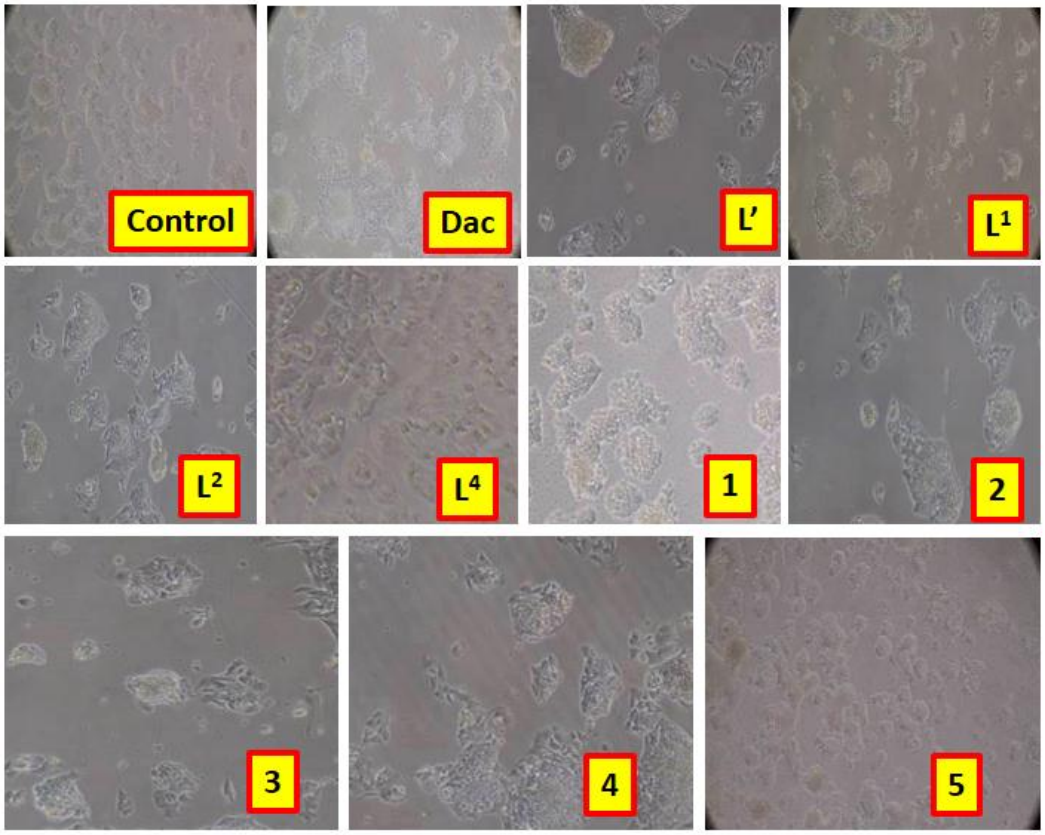

Fig. 6. Phase Contrast images of Hep G2 cells exposed to the potential compounds **Dac, L^1, L^2, L^4**, **1**, **2**, **3, 4** and **5** compared to the control indicating the *in-vitro* cytotoxic activity. These compounds were assayed at their respective *in-vitro* growth inhibitory IC_{50} value, as determined using the MTT assay in Hep G2 cells.

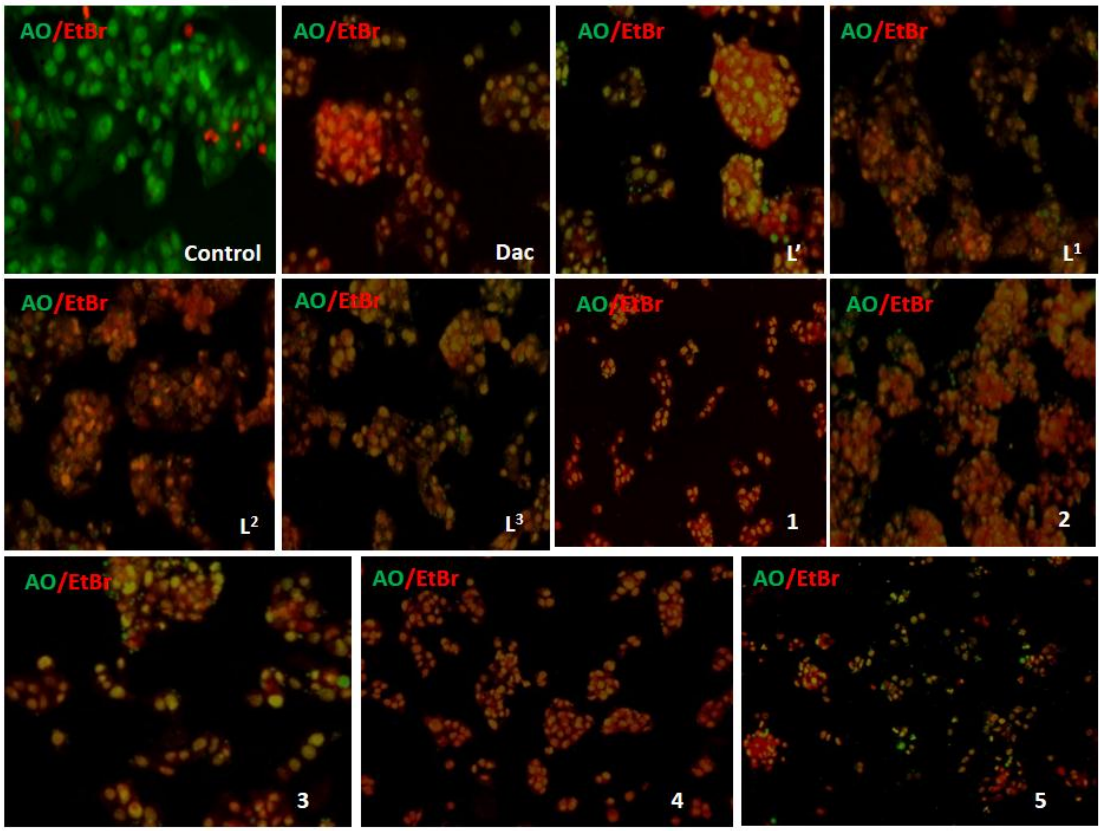

Fig. 7. Acridine Orange (AO)-Ethidium Bromide (EB) staining for detection of live and Apoptotic cells-Green denotes live cells with AO stained cells while red dented apoptotic cells stained with EB

The shrinking of cells,[53] is clearly visualised in the phase contrast images (Fig. 6) and supplemented further by acridine orange/ethidium bromide (AO/EB) staining which discriminates between viable, apoptotic and necrotic cells and marks nuclear changes (Fig. 7). **Dac**, **L^1**, **L^2**, **1**, **2**, **3**, **L'**, **L^4**, **4** and **5** were successfully stained for AO/EB, where the green fluorescence appears due to the viable cells stained by AO whereas the orange to red fluorescence with condensed chromatin[52] indicates apoptotic cells stained by EB. The exact mechanism and pathway of apoptosis can be elucidated by these interpretations.

6.4. Conclusion

The positive outcomes of our ongoing exploration in designing and syntheses of transition and organometallic based drugs [28, 30, 31] revealing noteworthy cytotoxic activity and reports on organotins as imminent biologically active metallopharmaceuticals [10-12] enthused us to develop a new series of diphenyltin^{IV} dithiocarbamate complexes $[(Ph_2Sn^{IV})_2$-μ^2-bis{(κ^2S,S-$S_2CN(R)CH_2CONHC_6H_4)_2SO_2$}] {R = Cy (**1**), ^{i}Pr (**2**), ^{n}Bu (**3**)} and $[(Ph_2Sn^{IV})_2$-μ^2-bis{(κ^2S,S-$S_2CN(R)CH_2CONH)_2C_6H_4$}] {R = Cy (**4**), ^{i}Pr (**5**)}. All these compounds were studied in depth and structurally characterized by FT-IR, MS, ^{1}H, ^{13}C and ^{1}H DOSY NMR spectroscopy, UV-visible, fluorescence spectrophotometers and by thermogravimetric analysis. Their *in vitro* cytotoxic activity against malignant human tumor Hep G2 (hepatoma) cell line was successfully studied by carrying out MTT assay for malignant human tumor Hep G2 (hepatoma) cell line. As reported by us previously, the chloro derivatives **Dac** [14.40 ± 0.83 µM], **L'** [12.68 ± 0.38 µM] of the lead compound Dapsone (**Dap**) and phenylene (**P**) showed 5 fold enhanced cytotoxicity compared to commonly used antineoplastic drug cisplatin (**C**). However in their repective diamine precursors which only $\mathbf{L^2}$ maintained the enhanced 5 fold cytotoxicity whereas, $\mathbf{L^1}$, and $\mathbf{L^3}$ showed comparable activity to cisplatin. Further as anticipated the cytotoxic activity of their corresponding binuclear organotin^{IV} dithiocarbamate complexes **1-5** was boosted exceptionally to as high as 22 fold in **1** [3.32 ± 0.14 µM], 44 fold in **2** [1.77 ± 0.11 µM], 37 fold in **3** [2.02 ± 0.47 µM], 8 fold in **4** [8.72 ± 0.19 µM] and 29 fold in **5** [2.60 ± 0.67µM] compared to reference drug cisplatin [75.67 ± 0.51 µM]. Exceptional cytotoxic activity of many of the organometallic derivatives opens the scope for further research against other carcinoma human cell types. Thorough mechanism and pathway of apoptosis is yet to be determined but morphological proofs like shrinking of cells specifies the induction of apoptosis as part of the mechanism of action of these compounds which is further reinforced by the individual staining of the cells by acridine orange/ethidium bromide (AO/EB). The findings here allows us to ascertain the simplicity of syntheses and fascinating *in vitro* cytotoxic activity in contrast to human cancer cell lines make the current series of organometallic binuclear Ph_2Sn^{IV} dithiocarbamate compounds capable for the forthcoming improvement of cytotoxic

agents. Thus, exceptional cytotoxic activity of many of the organometallic derivatives opens the scope for further research against other carcinoma human cell types.

6.5. References

[1] A. Alama, B. Tasso, F. Novelli, F. Sparatore, *Drug discovery today* **2009,** *14*, 500-508.

[2] Y. Jung, S. J. Lippard, *Chem. Rev*. **2007**, *107*, 1387–1407.

[3] G. J. M. Van der Kerk, J. G. A. Luijten, *J. Appl. Chem*. **1954**, *4*, 314-319.

[4] Cardarelli, N. E (**1976**). "Controlled-Release Pesticide Formulations." CRC Press, Cleveland, OH.

[5] J. Duncan, *Pharmacol. Ther*, **1980**, *10*, 407-429.

[6] N. J. Snoeij, A. H. Penninks, W. Seinen, *Environmental research*, **1987**, *44*, 335-353.

[7] M. Gielen, E.R.T. Tiekink, in: M. Gielen, E.R.T. Tiekink (Eds.), Tin Compounds and their Therapeutic Potential, in Metallotherapeutic Drugs and Metal-Based Diagnostic Agents: The Use of Metals in Medicine, John Wiley & Sons, Ltd., **2005**, p. 421.

[8] M. Gielen, Appl. Organomet. Chem. **2002**, *16*, 481.

[9] (a) M. Gielen, Coord. Chem. Rev. **1996**, *151*, 41, Gielen M (ed.); (b) Berlin, Springer Verlag, **1990**.

[10] S. Tabassum, C. Pettinari, *J. Organomet. Chem*. **2006**, *691*, 1761.

[11] C. Pellerito, P. D'Agati, T. Fiore, C. Mansueto, V. Mansueto, G. Stocco, L. Nagy, L. Pellerito, *J. Inorg. Biochem*. **2005**, *99*, 1294-1305.

[12] F. Cima, L. Ballarin, *Appl. Organomet. Chem*. **1999**, *13*, 697-703.

[13] P.J. Blower, Annu. *Rep. Prog. Chem., Sect. A.* **2004**, *100*, 633.

[14] A. Crowe, *J. Drugs Fut,* **1987**, *12*, 255–75.

[15] H.D. Yin, S.C. Xue, *Appl Organometa Chem*, **2006**, *20*, 283–289.

[16] O. Warburg, U¬ ber den Stoffwechsel der Tumouren; Springer: Berlin, **1926**.

[17] W. Friebolin, G. Schilling, M. Zöller, E. Amtmann, *J. Med. Chem*. **2005**, *48*, 7925-7931.

[18] V. Borghi, C. Porte, *Environ Sci Technol*, **2003**, *36*, 4224–4228.

[19] B. Pavoni et al, *Chimica e Industria*, **2005**, *87*, 44–52.

[20] L.N. Holloway et al, *Environ Toxicol Pharmacol*, **2008**, *25*, 43–50.

[21] G. Barone, T. Chaplin, T. G. Hibbert, A. T. Kana, M. F. Mahon, K. C. Molloy, I. D. Worsley, I. P. Parkin, L. S. Price, *Dalton Trans*. **2002**, 1085–1092.

[22] A. Torres-Huerta, B. Rodríguez-Molina, H. Höpfl, M. A. Garcia-Garibay, *Organometallics* **2014**, *33*, 354–362.

[23] D. C. Menezes, G. M. de Lima, F. A. Carvalho, M. G. Coelho, A. O. Porto, R. Augusti, J. D. Ardisson, *Appl. Organometal. Chem*. **2010**, *24*, 650–655.

[24] E. R. T. Tiekink, *CrystEngComm.* **2003**, *5*, 101–113.

[25] E. R. T. Tiekink, *Appl. Organometal. Chem*. **2008**, *22*, 533–550.

[26] N. Singh, S. Gupta, G. Nath, *Appl. Organometal. Chem*. **2000**, *14*, 484–492.

[27] D. C. Menezes, F. T. Vieira, G. M. de Lima, J. L. Wardell, M. E. Cortés, M. P. Ferreira, M. A. Soares, A. V. Boas, *Appl. Organometal. Chem*. **2008**, *22*, 221–226.

[28] R. Kadu, H. Roy, V. K. Singh, *Appl. Organomet. Chem*. **2015**, *29*, 746-755.

[29] V. K. Singh, R. Kadu, H. Roy, P. Raghavaiah, S. M. Mobin, *Dalton Trans.* **2015**, *45*, 1443-1454.

[30] V. Pillai, R. Kadu, L. Buch, V. K. Singh, *ChemistrySelect*. **2017**, *2*, 4382-4391.

[31] V. K. Singh, R. Kadu, H. Roy, *Eur. J. Med. Chem*. **2014**, *74*, 552-561.

[32] Manuscript under preparation…….

[33] R. Reyes-Martínez, R. Mejia-Huicochea, J. A. Guerrero-Alvarez, H. Höpfl, H. Tlahuext, *ARKIVOC* **2008**, part (v), 19–30.

[34] S. Leininger, B. Olenyuk, P. J. Stang, *Chem. Rev*. **2000**, *100*, 853–908.

[35] C. J. Jones, *Chem. Soc. Rev*. **1998**, *27*, 289–299.

[36] G. Ercolani, *J. Phys. Chem. B* **2003**, *107*, 5052–5057.

[37] H. L. Singh, A. K. Varshney, *Bioinorg. Chem. Appl*. **2006**, 23245.

[38] V. Barba, B. Arenaza, J. Guerrero, R. Reyes, *Heteroatom Chem*. **2012**, *23*, 422–428.

[39] J. P. Fuentes-Martínez, I. Toledo-Martínez, P. Román-Bravo, P. G. García, C. Godoy-Alcántar, M. López-Cardoso, H. Morales Rojas, *Polyhedron* **2009**, *28*, 3953–3966.

[40] R. Villamil-Ramos, A. K. Yatsimirsky, *Chem. Commun*. **2011**, *47*, 2694–2696.

[41] S. J. Blunden, P. J. Smith, *J. Organometal. Chem*. **1982**, *226*, 157–163.

[42] R. Sharma, N. K. Kaushik, *J. Therm. Anal Calorim*. **2004**, *78*, 953–964.

[43] A. Husain, S. A. A. Nami, K. S. Siddiqi, *Spectrochim. Acta A* **2009**, *73*, 89–95.

[44] R. Kadu, V. K. Singh, S. K. Verma, P. Raghavaiah, M. M. Shaikh, *J. Mol. Struct*. **2013**, *1033*, 298–311.

[45] N. A. Celis, R. Villamil-Ramos, H. Höpfl, I. F. Hernández-Ahuactzi, M. Sánchez, L. S. Zamudio-Rivera, V. Barba, *Eur. J. Inorg. Chem*. **2013**, 2912–2922.

[46] J. Cruz-Huerta, M. Carillo-Morales, E. Santacruz-Juárez, I. F. Hernández-Ahuactzi, J. Escalante-García, C. Godoy-Alcantar, J. A. Guerrero-Alvarez, H. Höpfl, H. Morales-Rojas, M. Sánchez, *Inorg. Chem*. **2008**, *47*, 9874–9885.

[47] S. R. Gadre, P. K. Bhadane, *Resonance* **1999**, *4*, 8–19.

[48] F. A. Bulat, A. Torro-Labbé, T. Brinck, J. S. Murray, P. Politzer, *J. Mol. Model*. **2010**, *16*, 1679–1691.

[49] P. Politzer, P. R. Laurence, K. Jayasuriya, *Environ. Health Perspect*. **1985**, *61*, 191–202.

[50] K. Liu, P. C. Liu, R. Liu, X. Wu, *Medical science monitor basic research*, **2015**, *21*, 15.

[51] S. K. Hadjikakou, N. Hadjiliadis, *Coordination Chemistry Reviews*, **2009**, *253*, 235-249.

[52] T. V. Berghe, S. Grootjans, V. Goossens, Y. Dondelinger, D. V. Krysko, N. Takahashi, P. Vandenabeele, *Methods*, **2013**, *61*, 117-129.

[53] Kasibhatla, S., Amarante-Mendes, G. P., Finucane, D., Brunner, T., Bossy-Wetzel, E., & Green, D. R. (**2006)**. Acridine orange/ethidium bromide (AO/EB) staining to detect apoptosis. Cold Spring Harbor Protocols, 2006(3), pdb-prot4493.

6.6. Annexures:

6.6.1. Spectral Characterization

Mass Spectra:

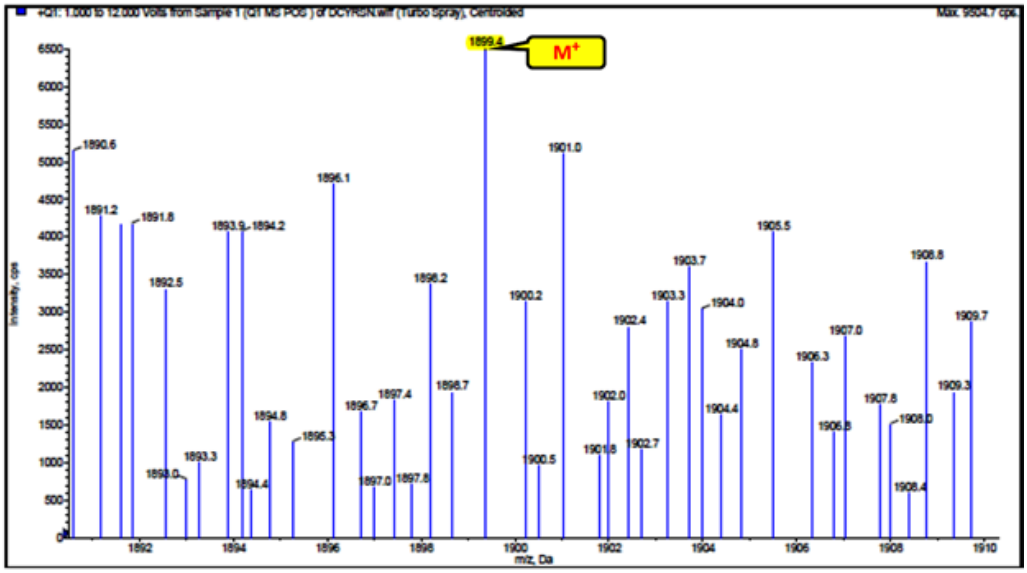

Annexure 1. Mass spectrum of **1**

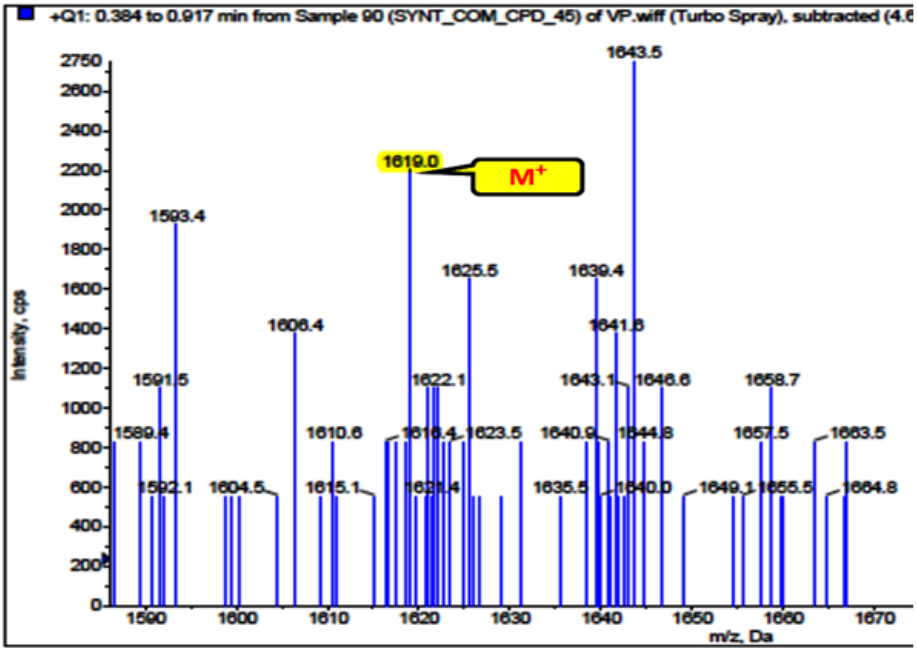

Annexure 2. Mass spectrum of **4**

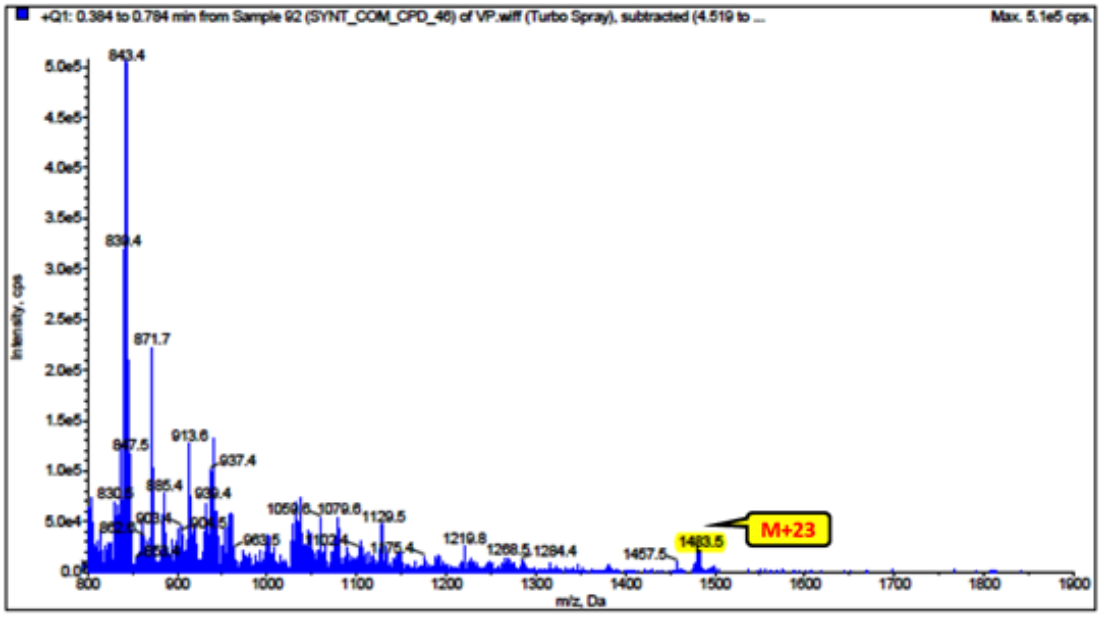

Annexure 3. Mass spectrum of **5**

IR spectral data:

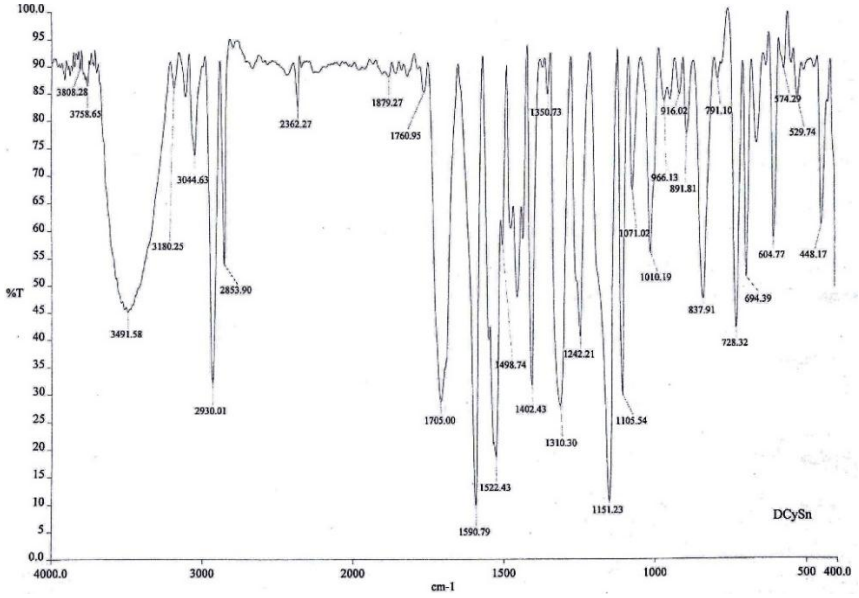

Annexure 4. IR spectra of **1**

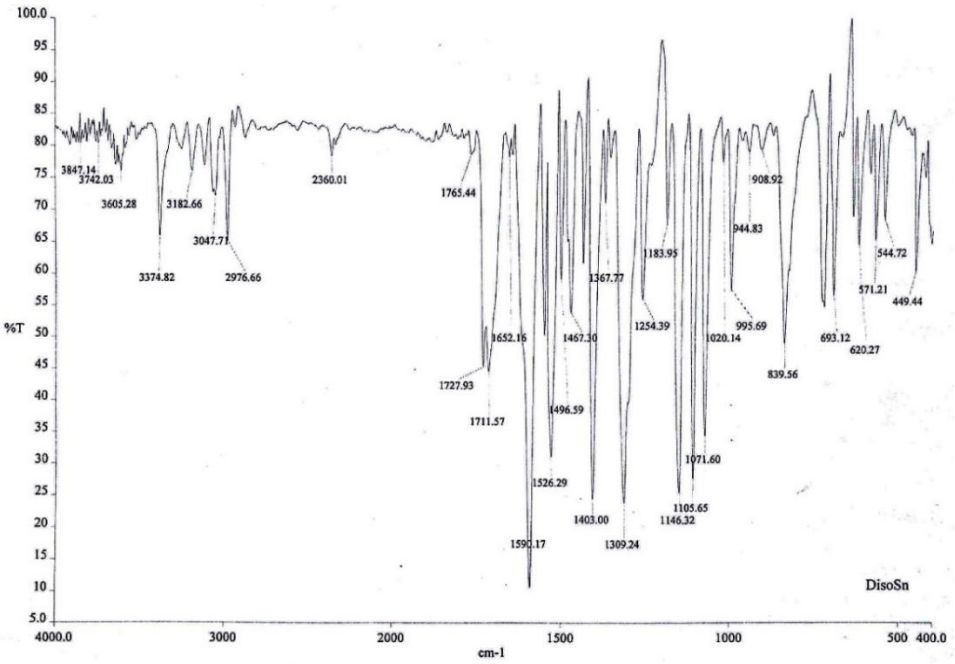

Annexure 5. IR spectra of **2**

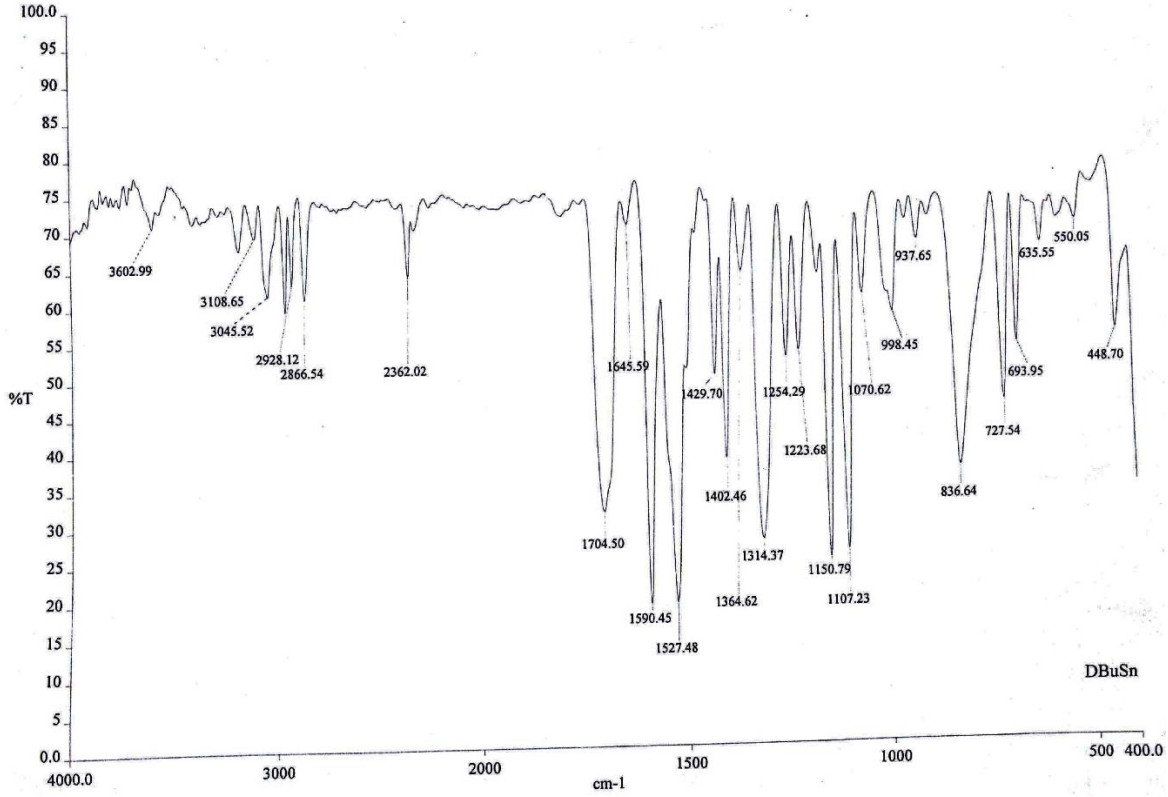

Annexure 6. IR spectra of **3**

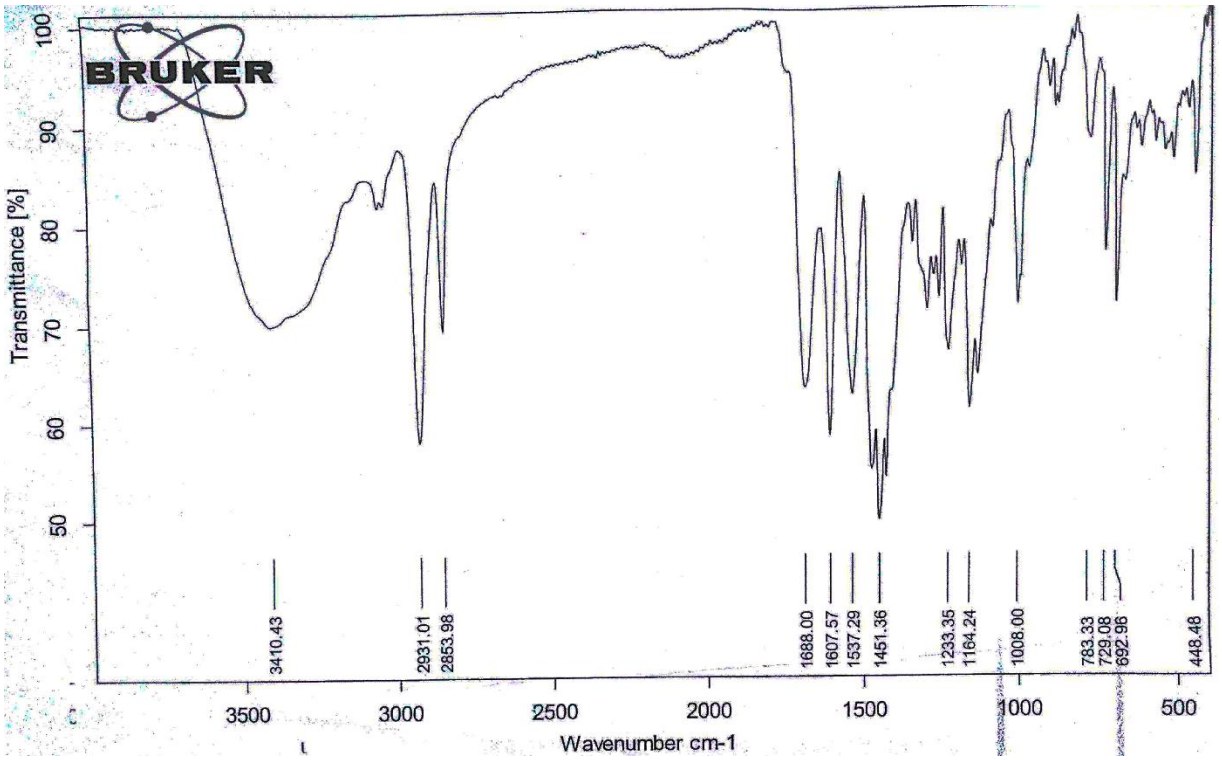

Annexure 7. IR spectra of **4**

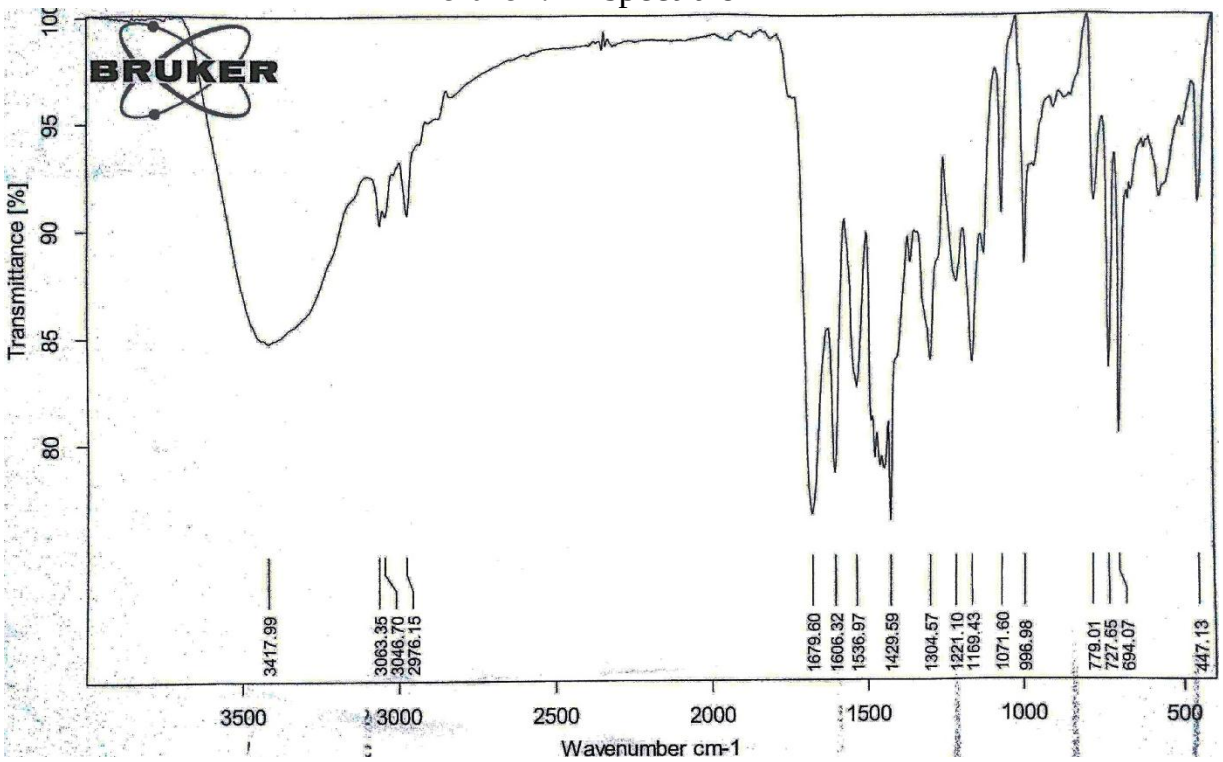

Annexure 8. IR spectra of **5**

NMR spectral data:

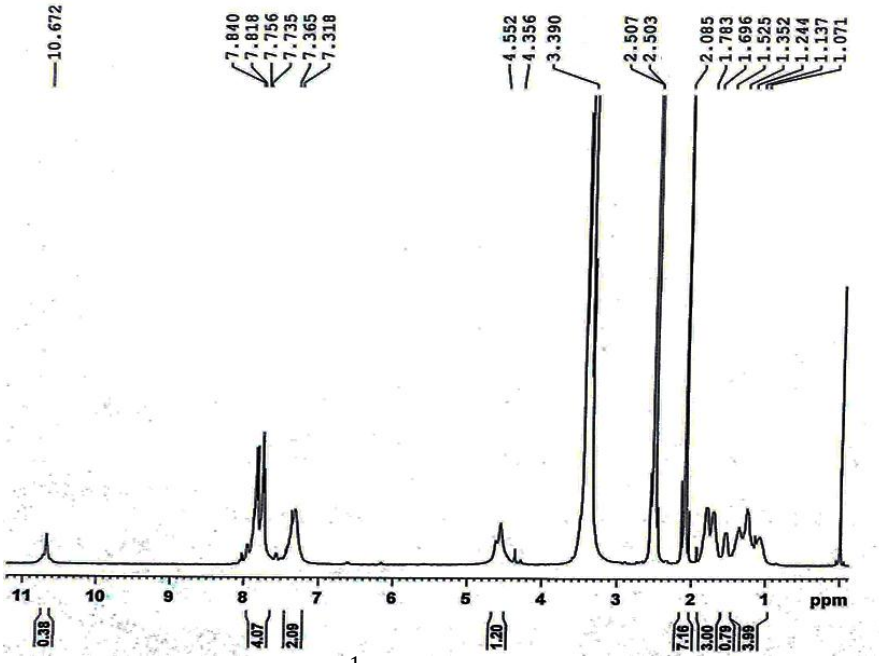

Annexure 9. ^{1}H NMR spectrum of **(1)**

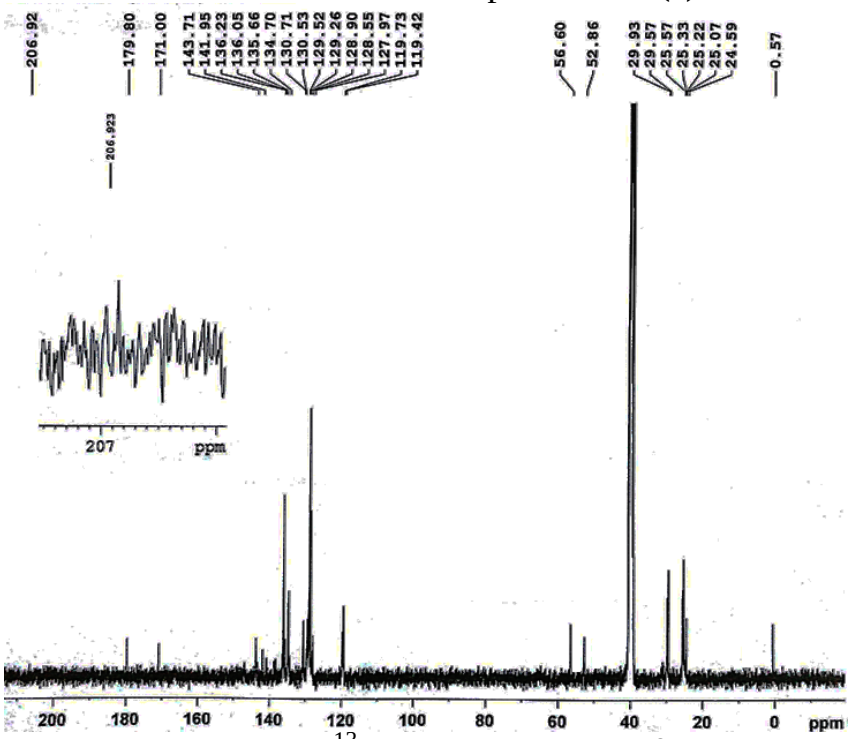

Annexure 10. ^{13}C NMR spectrum of **(1)**

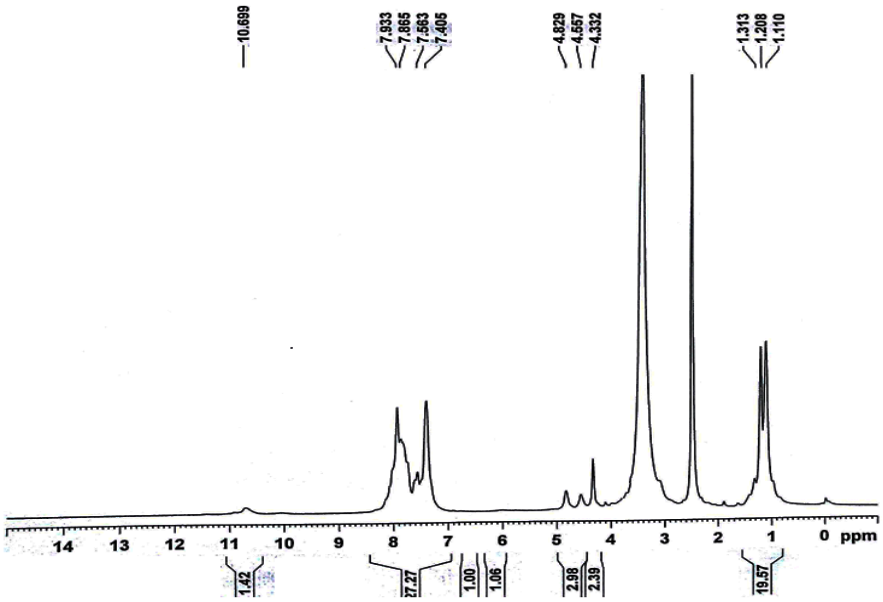

Annexure 11. ^{1}H NMR spectrum of **(2)**

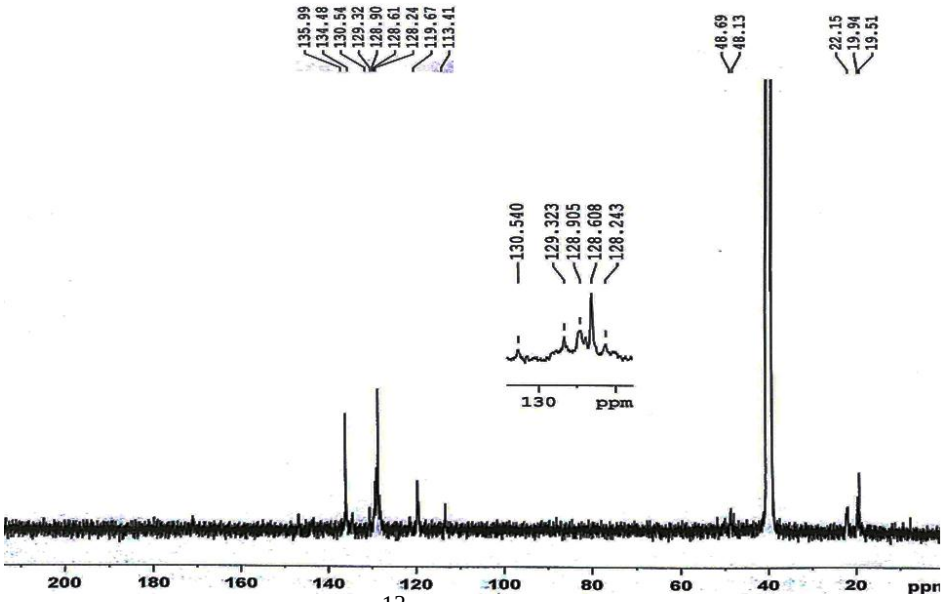

Annexure 12. ^{13}C NMR spectrum of **(2)**

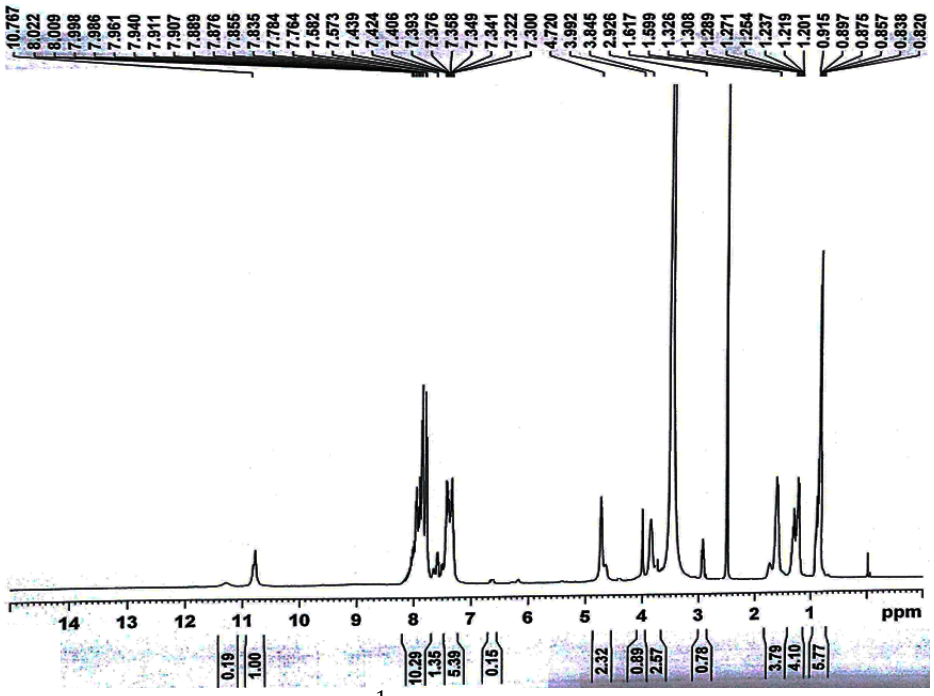

Annexure 13. ^{1}H NMR spectrum of **(3)**

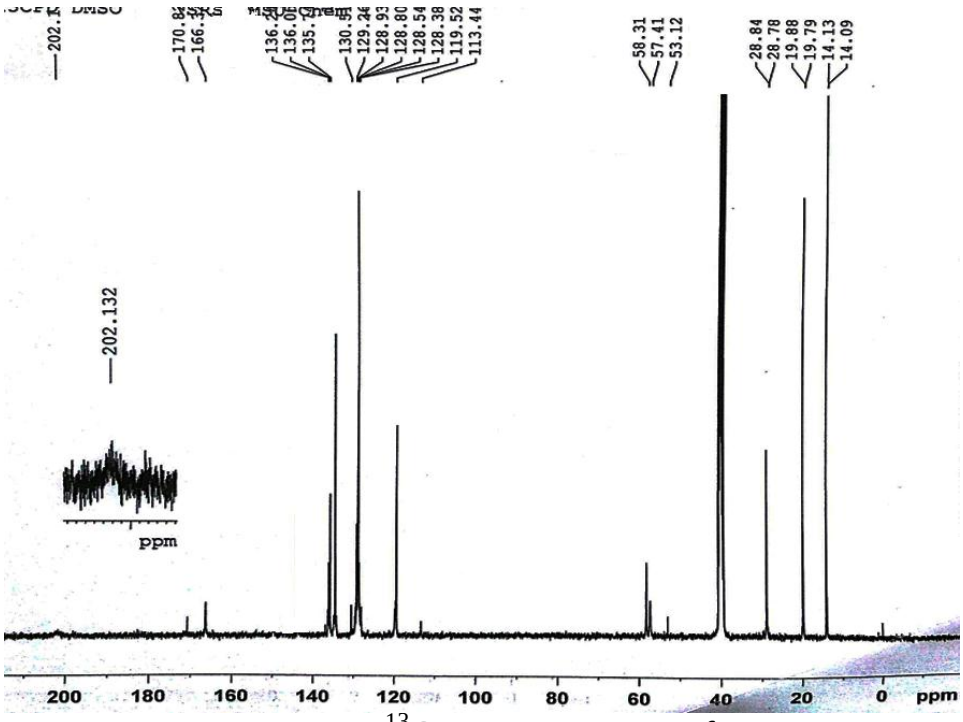

Annexure 14. ^{13}C NMR spectrum of **(3)**

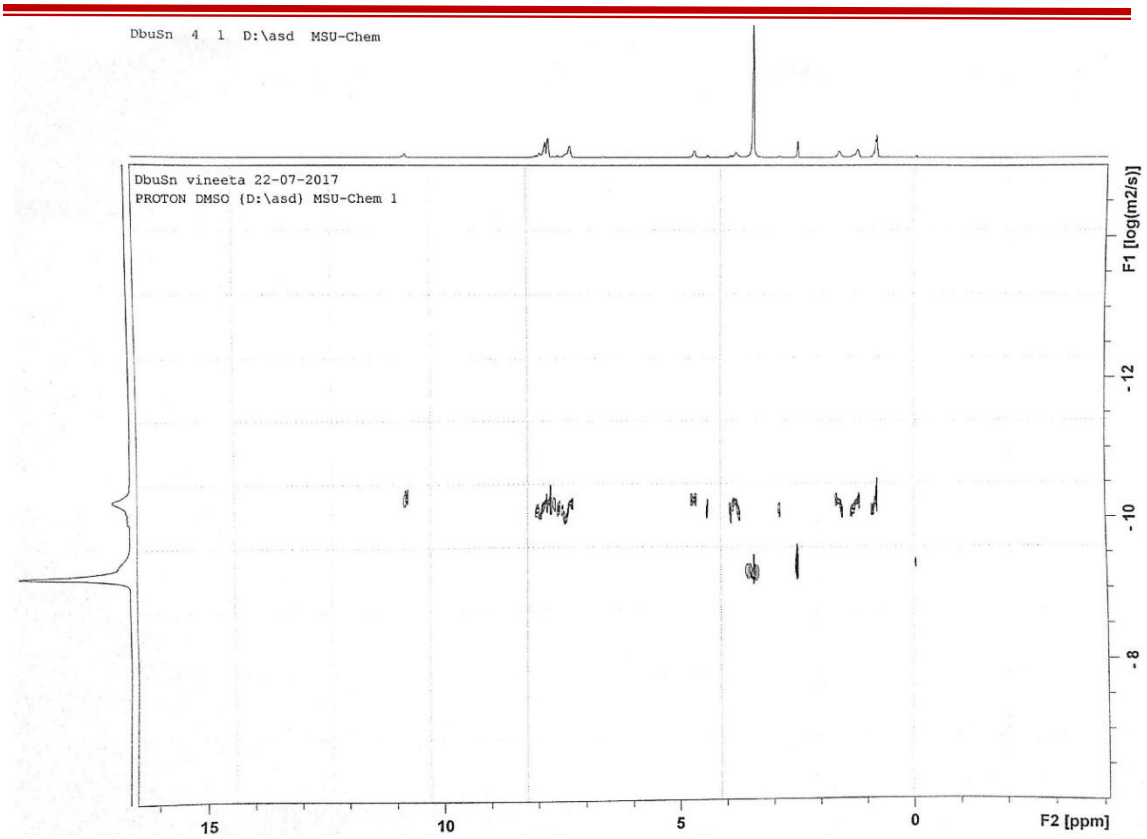

Annexure 15.DOSY NMR of **3**

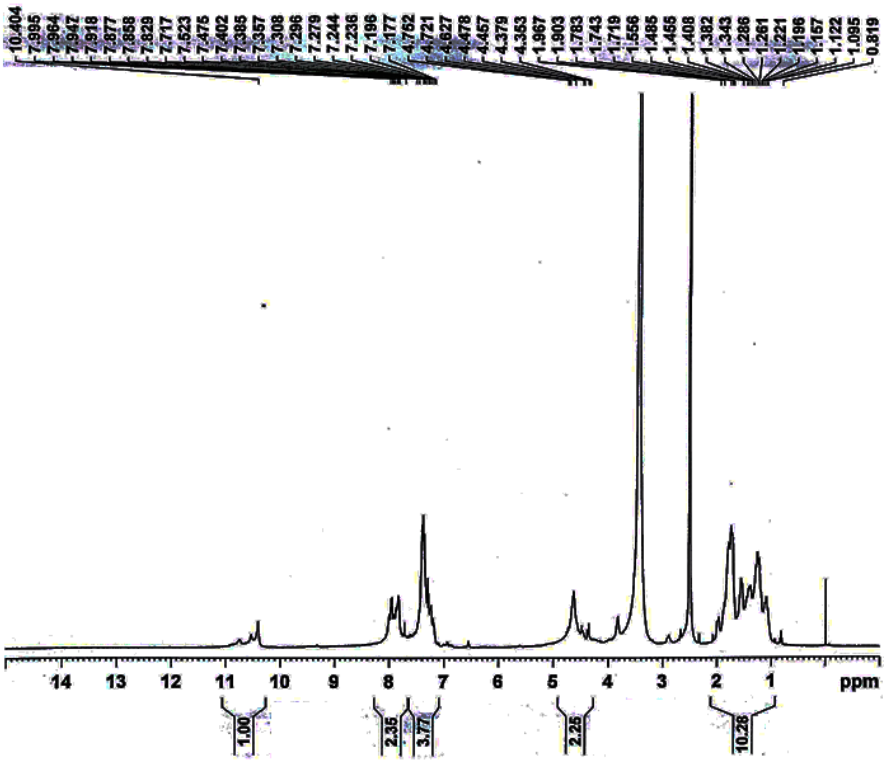

Annexure 16.^{1}H NMR spectrum of **(4)**

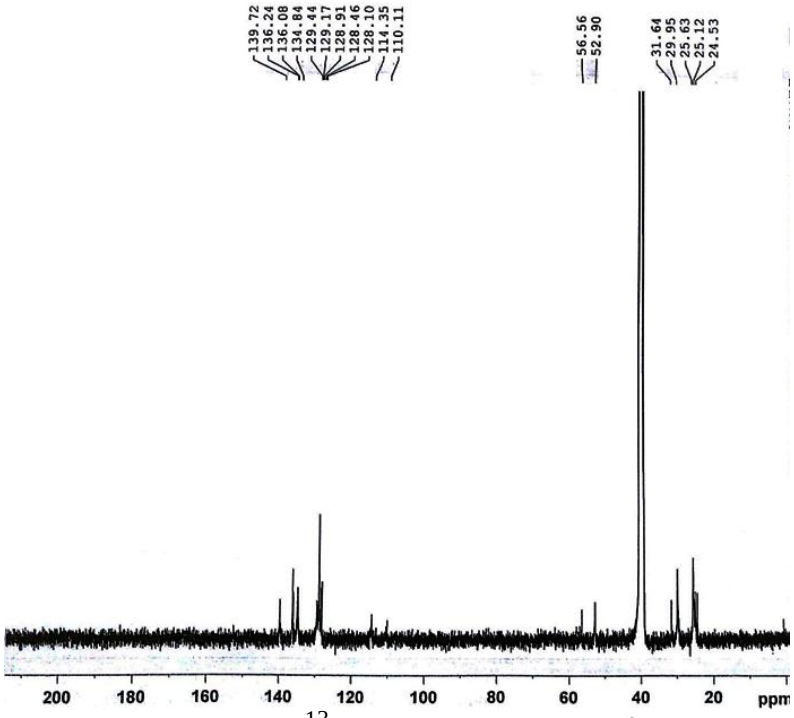

Annexure 17. ^{13}C NMR spectrum of **(4)**

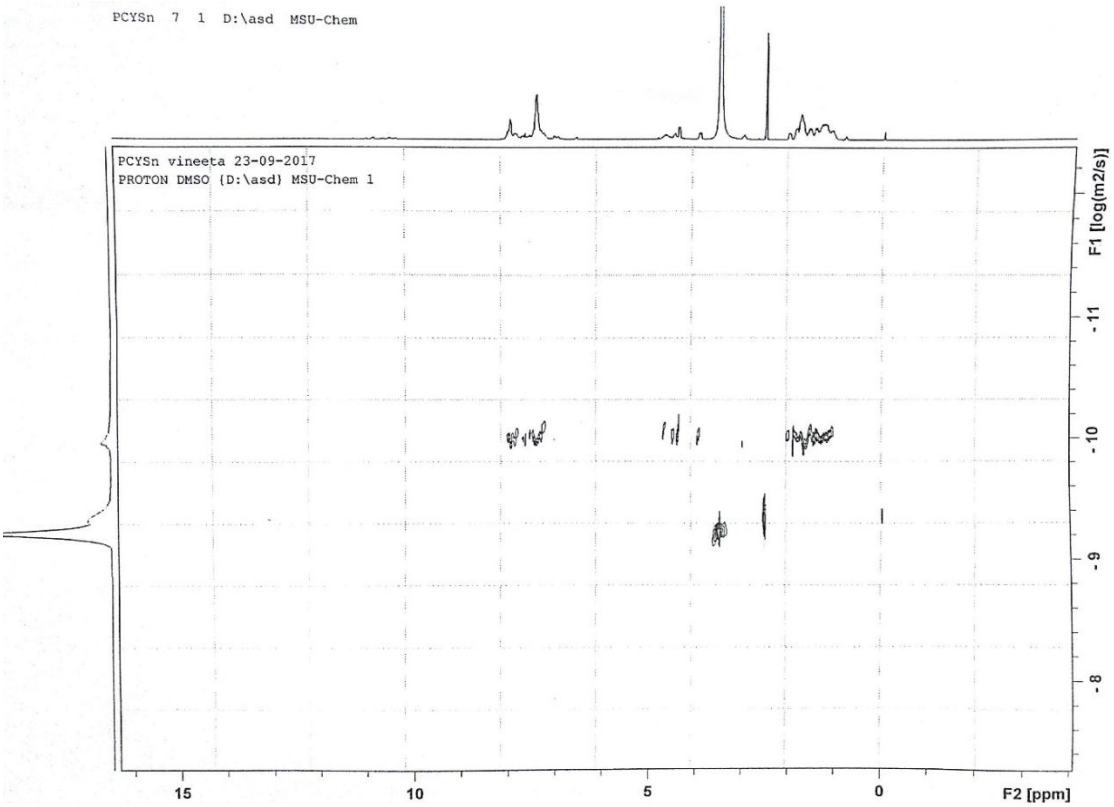

Annexure 18. DOSY NMR of **4**

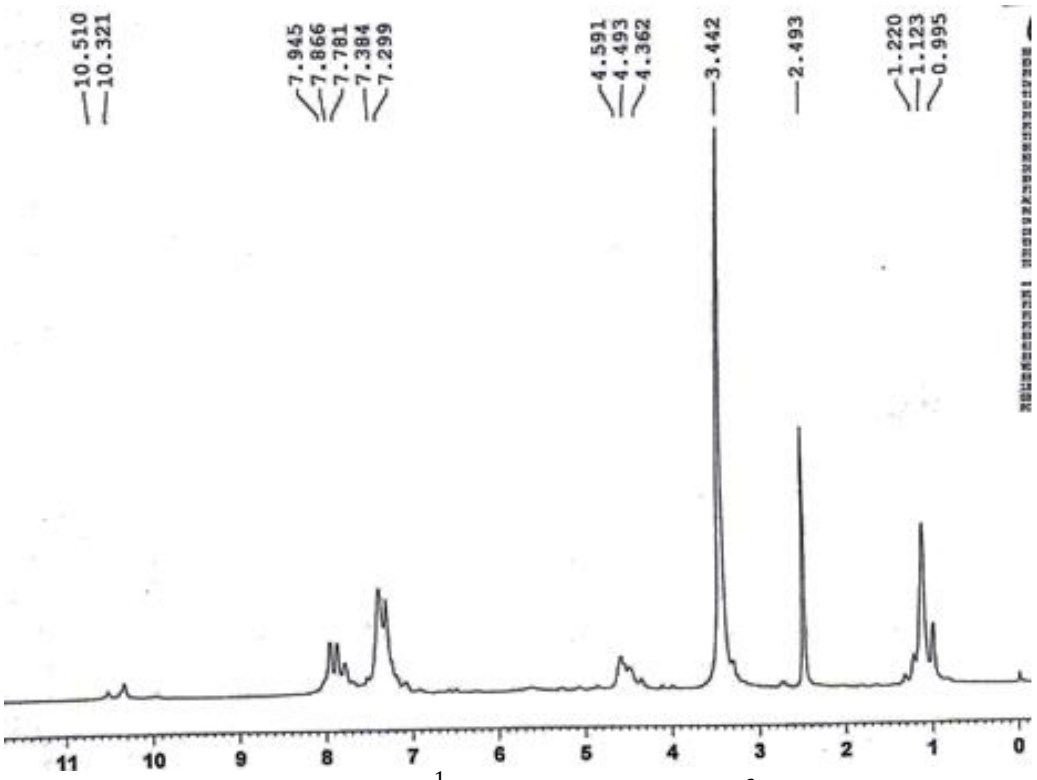

Annexure 19. ^{1}H NMR spectrum of **(5)**

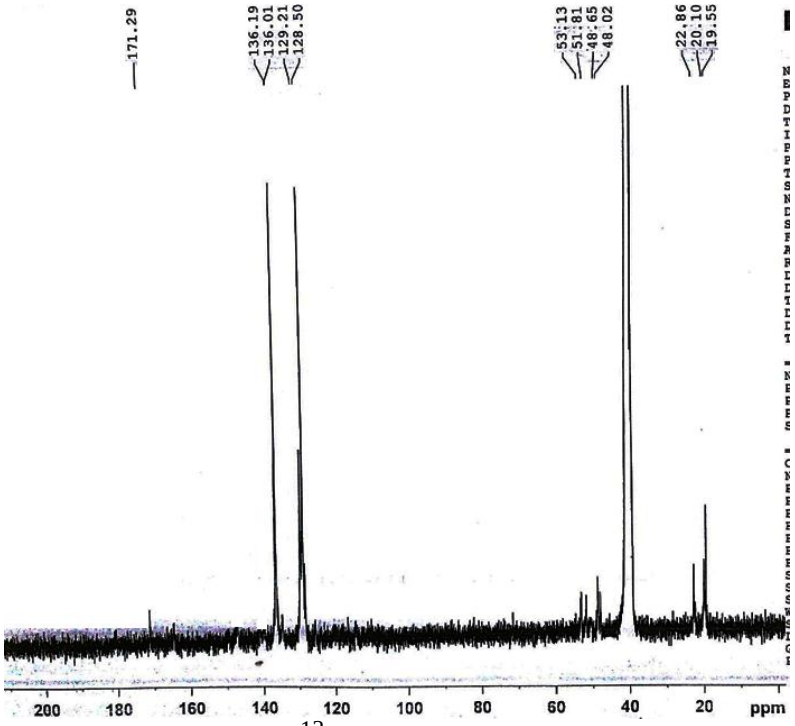

Annexure 20. ^{13}C NMR spectrum of **(5)**

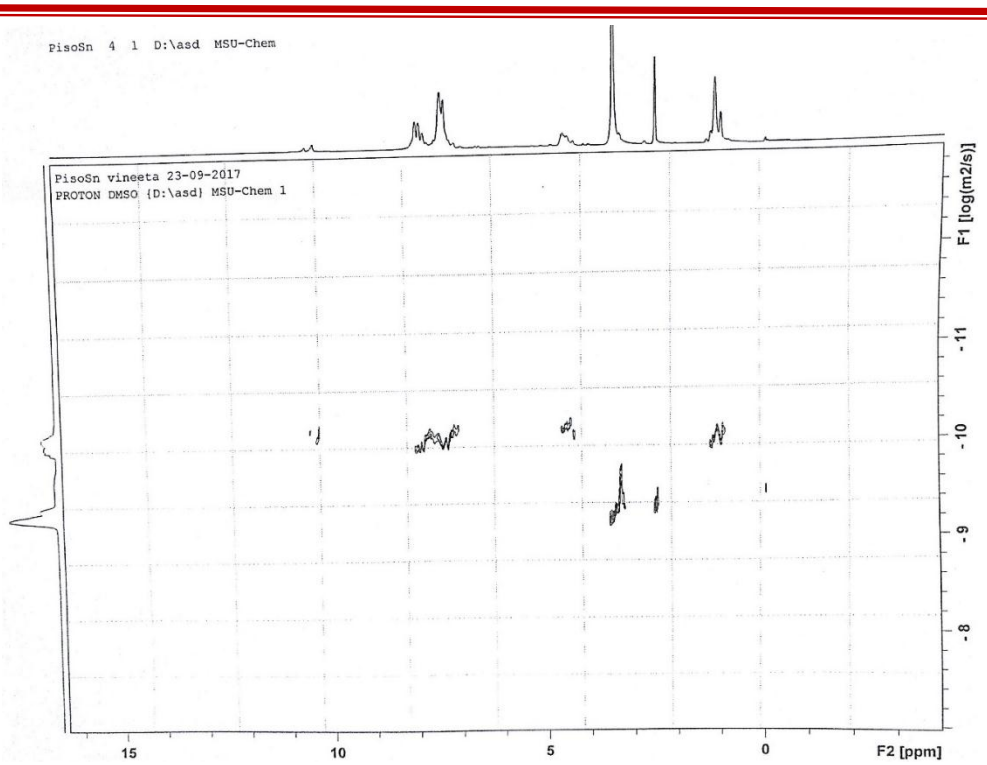

Annexure 21. DOSY NMR of **5**

Thermogravimetric Analysis

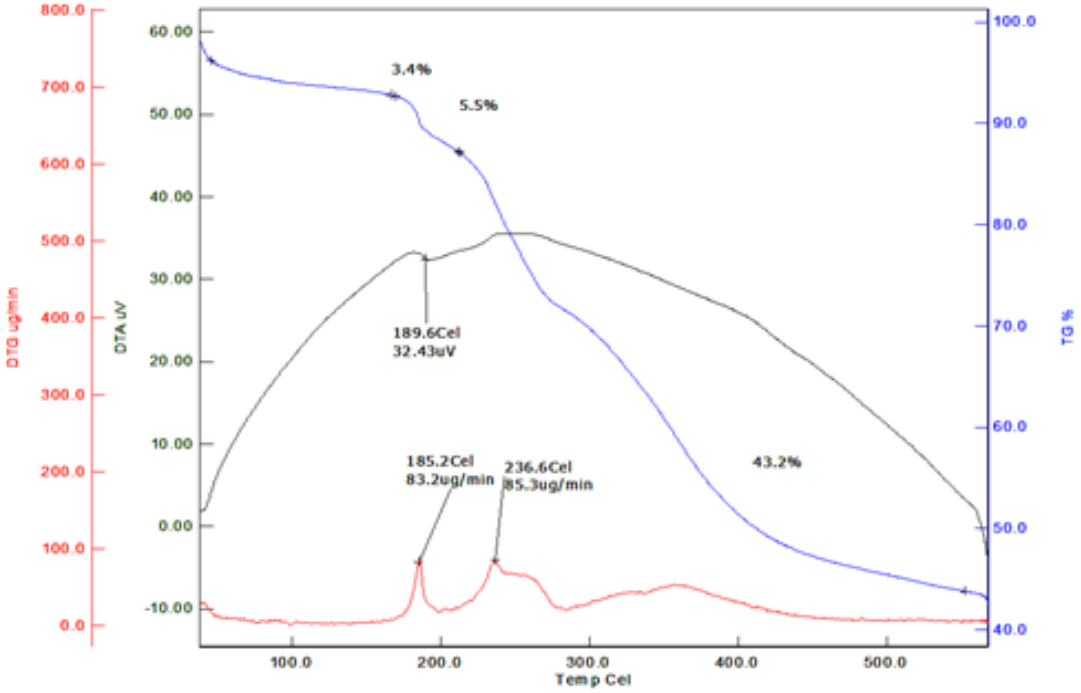

Annexure 22. TGA plot of **1**

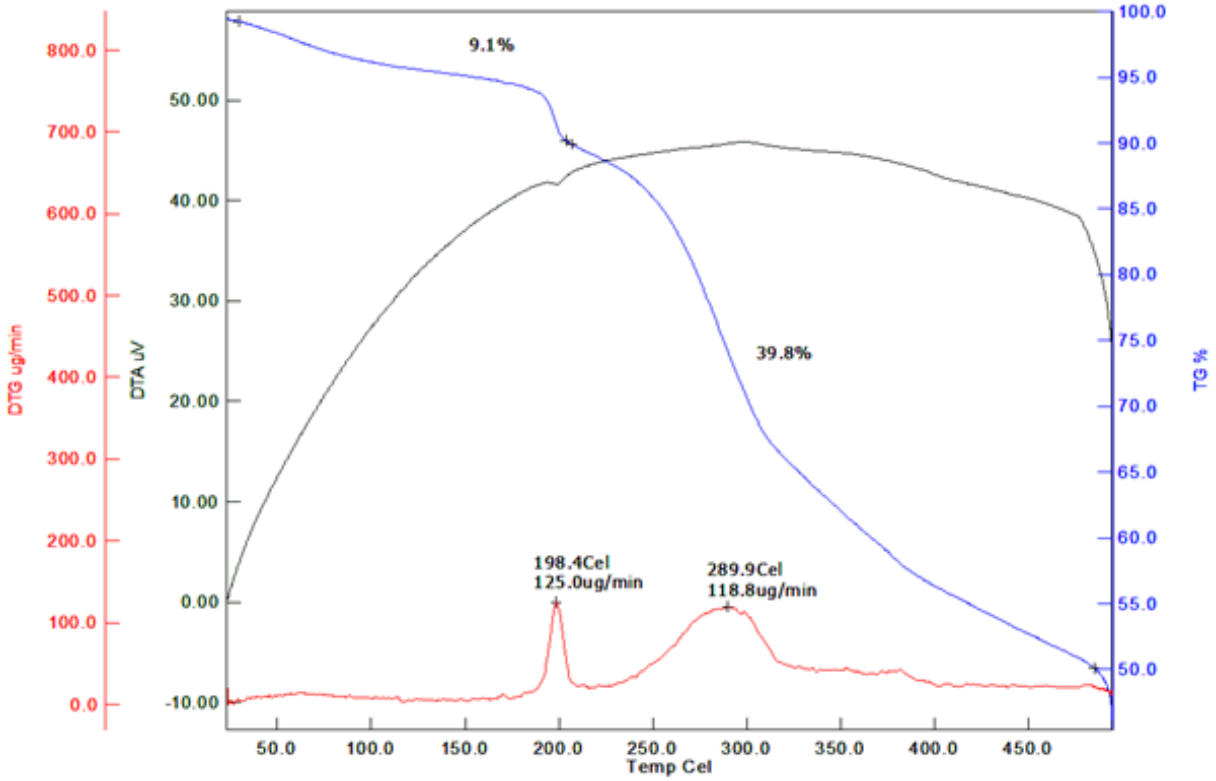

Annexure 23. TGA plot of **3**

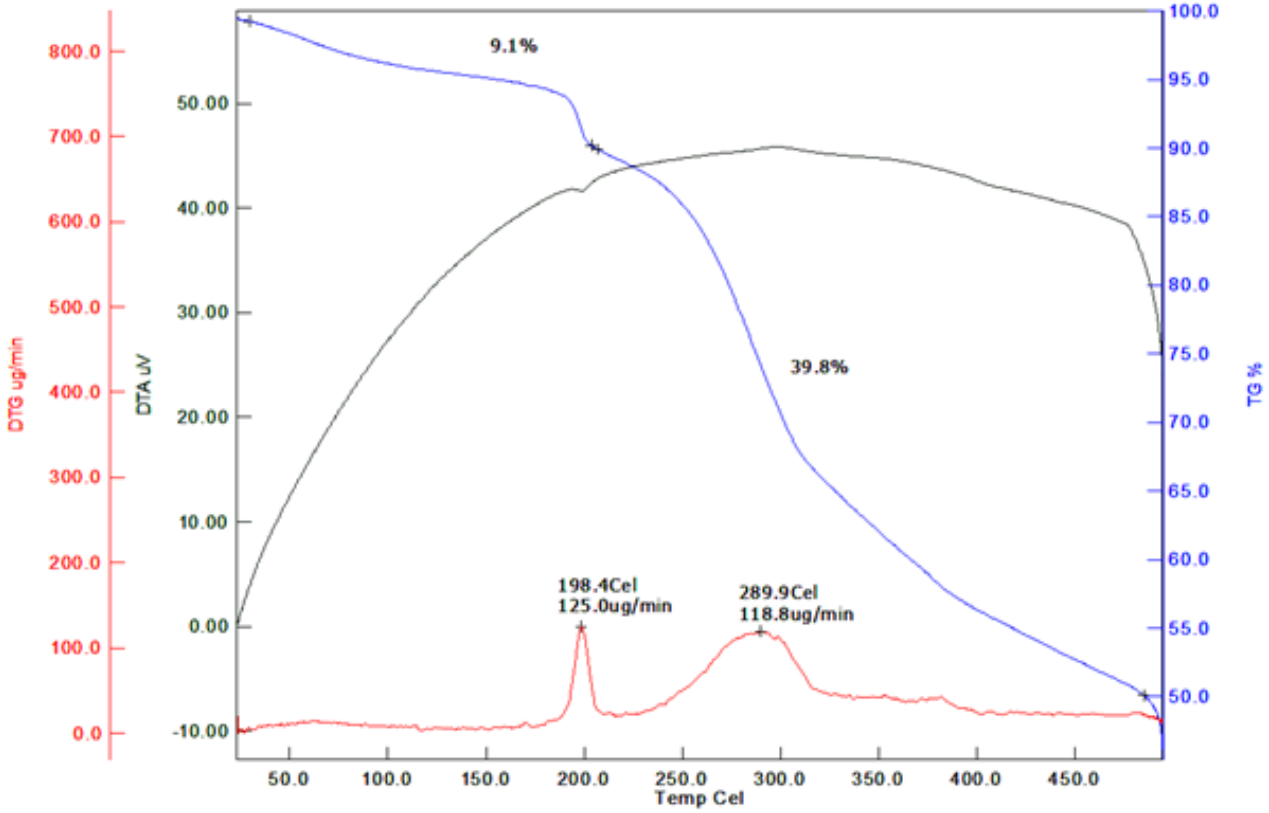

Annexure 24. TGA plot of **4**

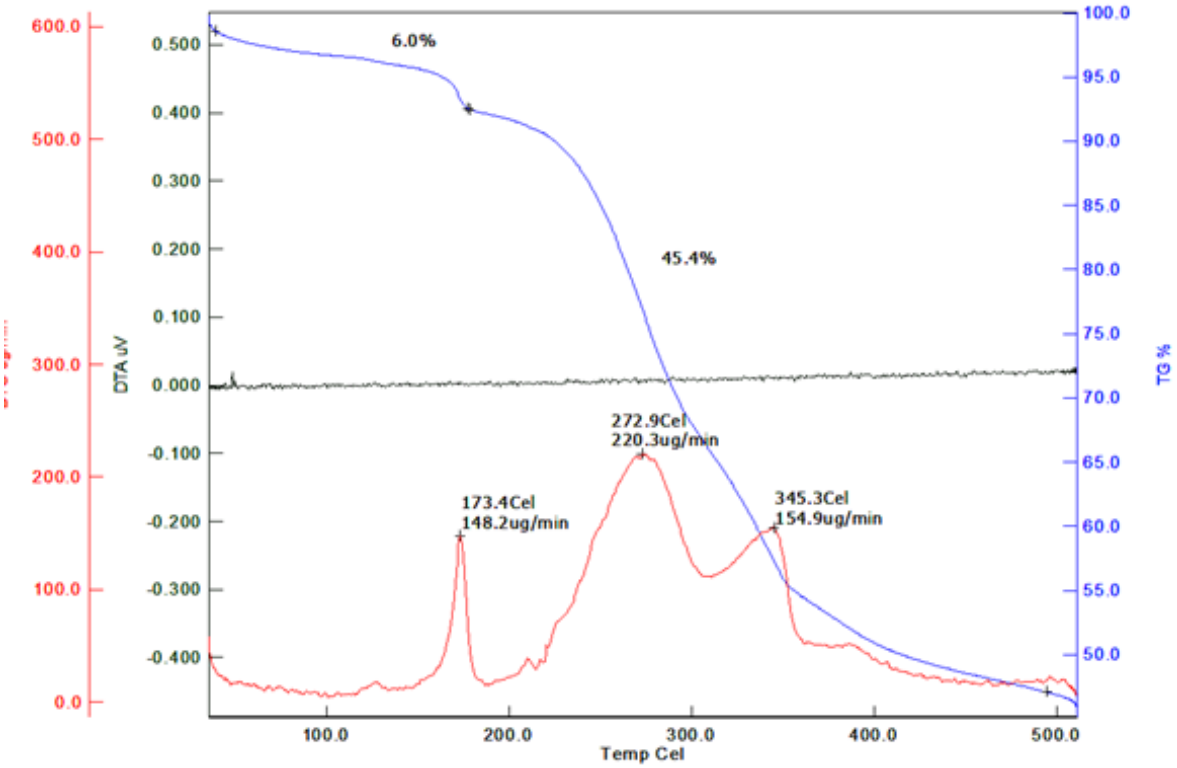

Annexure 25. TGA plot of **5**

This part of work is under communication: Manuscript ID: AOC-17-0760

The additional supporting Information related to this chapter is provided in the CD as follows:

Chapter 6

1. IR Spectra: **Table 1**
2. Thermogravimetric analysis: **Table 2**
3. In vitro cytotoxic study: **Table 3-4 and figure 1-3**
4. Geometry Optimization: **Table 5**
5. References